The Astrophysical Journal Supplement Series, 172:523–544, 2007 September

Lyα EMITTERS AT REDSHIFT 5.7 IN THE COSMOS FIELD[1]

T. Murayama,[2] Y. Taniguchi,[3] N. Z. Scoville,[4,5] M. Ajiki,[2] D. B. Sanders,[5] B. Mobasher,[6] H. Aussel,[5,7] P. Capak,[4] A. Koekemoer,[6] Y. Shioya,[3] T. Nagao,[8,9] C. Carilli,[10] R. S. Ellis,[4] B. Garilli,[11] M. Giavalisco,[6] M. G. Kitzbichler,[12] O. Le Fèvre,[13] D. Maccagni,[11] E. Schinnerer,[14] V. Smolčić,[15,16] S. Tribiano,[17,18] A. Cimatti,[9] Y. Komiyama,[8] S. Miyazaki,[19] S. S. Sasaki,[2,4] J. Koda,[4] and H. Karoji[8]

Received 2006 September 21; accepted 2007 February 14

ABSTRACT

We present results from a narrowband optical survey of a contiguous area of 1.95 deg^2, covered by the Cosmic Evolution Survey (COSMOS). Both optical narrowband ($\lambda_c = 8150$ Å and $\Delta\lambda = 120$ Å) and broadband (B, V, g', r', i', and z') imaging observations were performed with the Subaru prime-focus camera, Suprime-Cam on the Subaru Telescope. We provide the largest contiguous narrowband survey, targeting Lyα emitters (LAEs) at $z \approx 5.7$. We find a total of 119 LAE candidates at $z \sim 5.7$. Over the wide-area covered by this survey, we find no strong evidence for large-scale clustering of LAEs. We estimate a star formation rate (SFR) density of $\sim 7 \times 10^{-4}\ M_\odot\ \mathrm{yr}^{-1}\ \mathrm{Mpc}^{-3}$ for LAEs at $z \approx 5.7$ and compare it with previous measurements.

Subject headings: cosmology: observations — early universe — galaxies: evolution — galaxies: formation

1. INTRODUCTION

Understanding of the formation and early evolution of galaxies requires study of rest-frame properties of well-defined samples of high-redshift galaxies. These are needed to address the cosmic star formation history and growth of large-scale structures in the early universe and the source of cosmic reionization of intergalactic space. There are two widely used techniques to select such high-redshift galaxies: (1) the Lyman break technique, aiming for Lyman break galaxies (LBGs; Steidel et al. 1999; Iwata et al. 2003; Ouchi et al. 2004; Bouwens & Illingworth 2006 and references therein), and (2) narrowband imaging surveys, targeting Lyα emitters (LAEs; Hu & McMahon 1996; Rhoads & Malhotra 2001; Ajiki et al. 2003; Hu et al. 2004; Taniguchi et al. 2005 and references therein). The narrowband surveys are mainly aimed at star-forming population while Lyman break technique also selects galaxies with older age.

Recently, LAE surveys have extended study of the clustering and morphology of star-forming galaxies to the highest redshifts (Shimasaku et al. 2004; Ouchi et al. 2005; Ajiki et al. 2006a). Indeed, some of the previous LAE surveys have shown signs of large-scale structures, either using two-dimensional projected distribution of galaxies or three-dimensional distribution, also using redshifts. For example, evidence for clustering of LAEs at $z \approx 4.9$ was found over an area of $\simeq 0.5^\circ \times 0.5^\circ$, covered by the Subaru Deep Field (SDF; Shimasaku et al. 2004; see also Ouchi et al. 2003), extending to ~ 20 Mpc $\times$ 50 Mpc. However, no such structures were found for LAEs at $z \approx 5.7$ (Shimasaku et al. 2006) and $z \approx 6.6$ (Taniguchi et al. 2005; Kashikawa et al. 2006). Although, using a spectroscopically confirmed sample of 34 LAEs at $z \approx 5.7$, Shimasaku et al. (2006) found evidence for weak clustering. In an independent study, using a spectroscopically confirmed sample of 19 LAEs at $z \approx 5.7$, Hu et al. (2004) found structures extending to angular scales of $\sim$60 Mpc with evidence for filamentary structures. This result was further confirmed by Ouchi et al. (2005), who found filamentary structures of size 10–40 Mpc in the Subaru *XMM-Newton* Deep Survey (SXDS; Sekiguchi et al. 2004), using a photometric sample of 515 LAEs. In addition to the above results, based on deep narrowband surveys in so-called "blank fields," evidence has been accumulating in support of clustering at $z = 4.1$–5.2, with a few Mpc scales around high-redshift radio galaxies (Venemans et al. 2002, 2004; Overzier et al. 2006) and quasar SDSS J0836+0054 (Zheng et al. 2006; Ajiki et al. 2006b).

These studies are useful in investigating early formation of galaxies and large-scale structures. Furthermore, they provide important constraints on both the star formation and cosmic reionization history. A detailed study of clustering of galaxies at high redshifts requires deep and wide-area surveys to allow a homogeneously selected sample of galaxies and to minimize effects of cosmic variance. This is the subject of the present paper.

In this paper we present the largest survey of LAEs at $z \approx 5.7$, covering the entire 2 square degree field of the Cosmic Evolution

[1] Based on data collected at the Subaru Telescope, which is operated by the National Astronomical Observatory of Japan.

[2] Astronomical Institute, Graduate School of Science, Tohoku University, Aramaki, Aoba, Sendai 980-8578, Japan.
[3] Physics Department, Graduate School of Science and Engineering, Ehime University, 2-5 Bunkyo-cho, Matsuyama 790-8577, Japan.
[4] Department of Astronomy, MS 105-24, California Institute of Technology, Pasadena, CA 91125.
[5] Institute for Astronomy, University of Hawaii, 2680 Woodlawn Drive, Honolulu, HI 96822.
[6] Space Telescope Science Institute, 3700 San Martin Drive, Baltimore, MD 21218.
[7] CEA Saclay, DSM/DAPNIA/SAp, 91191 Gif-sur-Yvette Cedex, France.
[8] National Astronomical Observatory of Japan, 2-21-1, Osawa, Mitaka, Tokyo 181-8588, Japan.
[9] INAF—Osservatorio Astrofisico di Arcetri, Largo Enrico Fermi 5, 50125 Firenze, Italy.
[10] National Radio Astronomy Observatory, P.O. Box O, Socorro, NM 87801-0387.
[11] INAF, Istituto di Astrofisica Spaziale e Fisica Cosmica, Sezione di Milano, via Bassini 15, 20133 Milano, Italy.
[12] Max-Planck-Institut für Astrophysik, D-85748 Garching bei München, Germany.
[13] Laboratoire d'Astrophysique de Marseille, BP 8, Traverse du Siphon, 13376 Marseille Cedex 12, France.
[14] Max Planck Institut für Astronomie, Königstuhl 17, Heidelberg, D-69117, Germany.
[15] Princeton University Observatory, Princeton, NJ 08544.
[16] University of Zagreb, Department of Physics, Bijenicka cesta 32, 10000 Zagreb, Croatia.
[17] American Museum of Natural History.
[18] CUNY Bronx Community College, New York, NY.
[19] Subaru Telescope, National Astronomical Observatory of Japan, 650 North A'ohoku Place, Hilo, HI 96720.

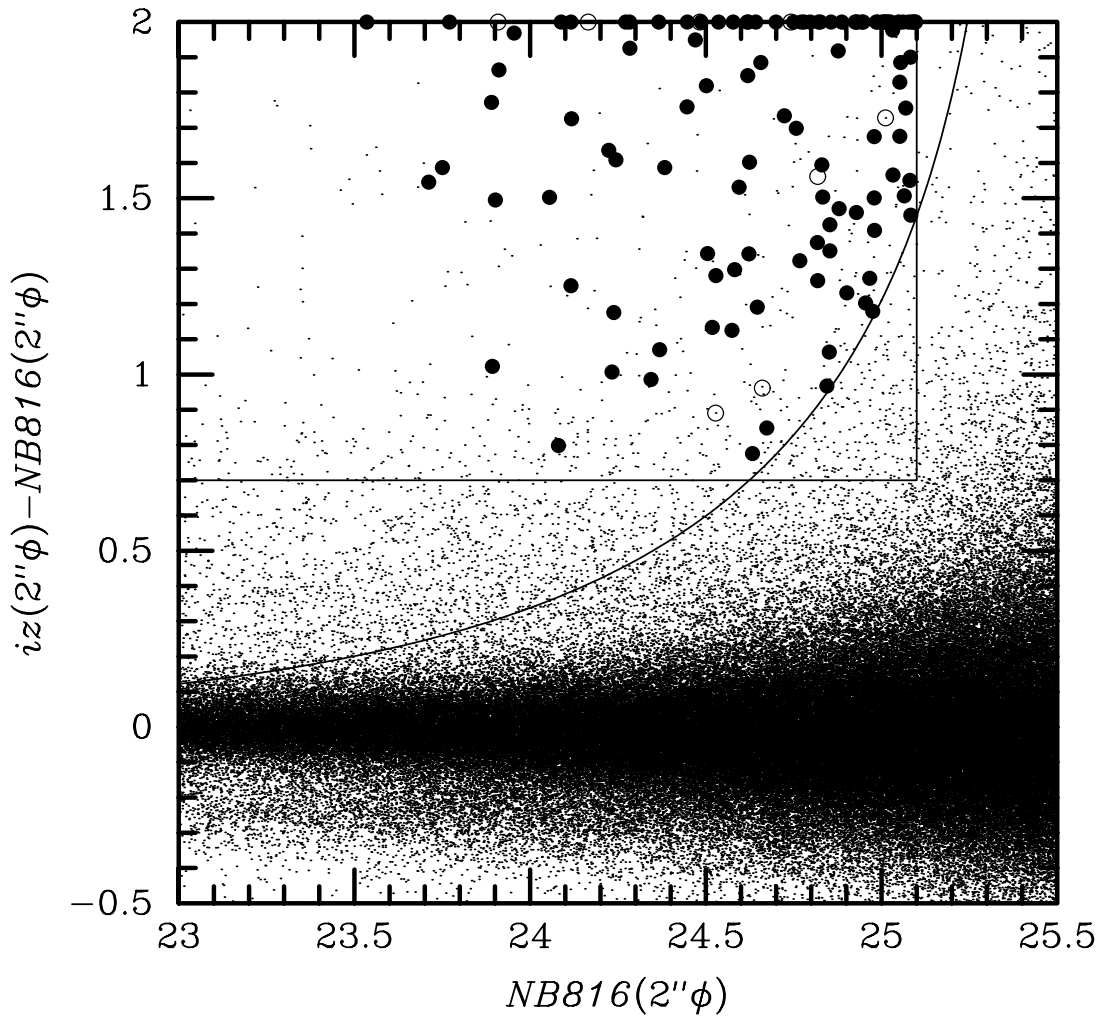

FIG. 1.—Diagram between $iz - \mathrm{NB816}$ and NB816 for all objects detected with $\mathrm{NB816} < 26$. Our LAE candidates are shown by filled circles (the statistical sample) and open circles (the nonstatistical sample). Objects with $iz - \mathrm{NB816} > 2$ are shown at $iz - \mathrm{NB816} = 2$ for clarity. The vertical line shows the detection limit of $\mathrm{NB816} = 25.1$. The horizontal line shows the selection criterion of $iz - \mathrm{NB816} = 0.7$. The curve shows the 3 σ limit for the $iz - \mathrm{NB816}$ color.

Survey (COSMOS), centered at $\alpha(\mathrm{J2000.0}) = 10^{\mathrm{h}}00^{\mathrm{m}}28.6^{\mathrm{s}}$ and $\delta(\mathrm{J2000.0}) = +02^{\circ}12'21.0''$ (Scoville et al. 2007). The full COSMOS field has been observed in I_{814} band with the Advanced Camera for Surveys (ACS) on board the *Hubble Space Telescope* (*HST*). In addition to the ACS data, the multiwavelength broad- and narrowband observations were also performed using the Supreme-Cam (Miyazaki et al. 2002) on the Subaru Telescope (Kaifu et al. 2000; Iye et al. 2004). The narrowband filter NB816 has an effective wavelength of $\lambda_c = 8150$ Å with a width $\Delta\lambda = 120$ Å (see Ajiki et al. 2003 for details), allowing to select LAEs in the range $5.65 < z < 5.75$. We assume standard cosmology with $\Omega_{\mathrm{matter}} = 0.3$, $\Omega_{\Lambda} = 0.7$, and $H_0 = 70$ km s^{-1} Mpc^{-1}. Throughout this paper, we use magnitudes in the AB system.

2. OBSERVATIONS AND SAMPLE SELECTION

2.1. *Data and Source Detection*

We carried out an optical narrowband (NB816) imaging survey of the entire 2 deg^2 area of the COSMOS field, using the Suprime-Cam on the Subaru Telescope. These observations, combined with the broadband (B, V, g', r', i', and z') Suprime-Cam and ACS (I_{814}) photometric data will be used to identify LAE candidates at $z \sim 5.7$ and to study their properties. Details of the narrowband and ground-based observations and data reduction are given in Taniguchi et al. (2007) and Capak et al. (2007) and for the *HST* ACS observations in Koekemoer et al. (2007).

For the ground-based observations, the seeing size varies between the exposures. The PSF size of each NB816 images is between 0.4″ and 0.7″. To optimize source detection in NB816, we only use exposures with PSF sizes smaller than 1.15″ to construct a combined image.

The limiting magnitude of the NB816 has a variance of ~0.5 mag, depending on the location on the image. We only confine our LAE search to areas with low noise where the 5 σ limiting magnitude with a 2″ diameter aperture in NB816 is ~25.1. This corresponds to a total effective area of 1.95 deg^2. The transverse comoving area of the LAE survey at $z = 5.7$ is 3.9×10^4 Mpc^2. The FWHM of the filter, which has a Gaussian-like shape, corresponds to a comoving depth of 45 Mpc, spanning the redshift range $5.65 < z < 5.75$ along the line of sight. Therefore, our NB816 survey probes a volume of 1.8×10^6 Mpc^3.

We have performed source detection and photometry on the NB816 image with SExtractor version 2.3 (Bertin & Arnouts 1996). A source is selected as a contiguous 9 pixel area above the 3 σ noise level (corresponding to 26.48 mag arcsec^{-2}) on the NB816 image. Photometry is performed on the NB816 and the broadband images over 0.5″, 2″, and 3″ diameter apertures. To

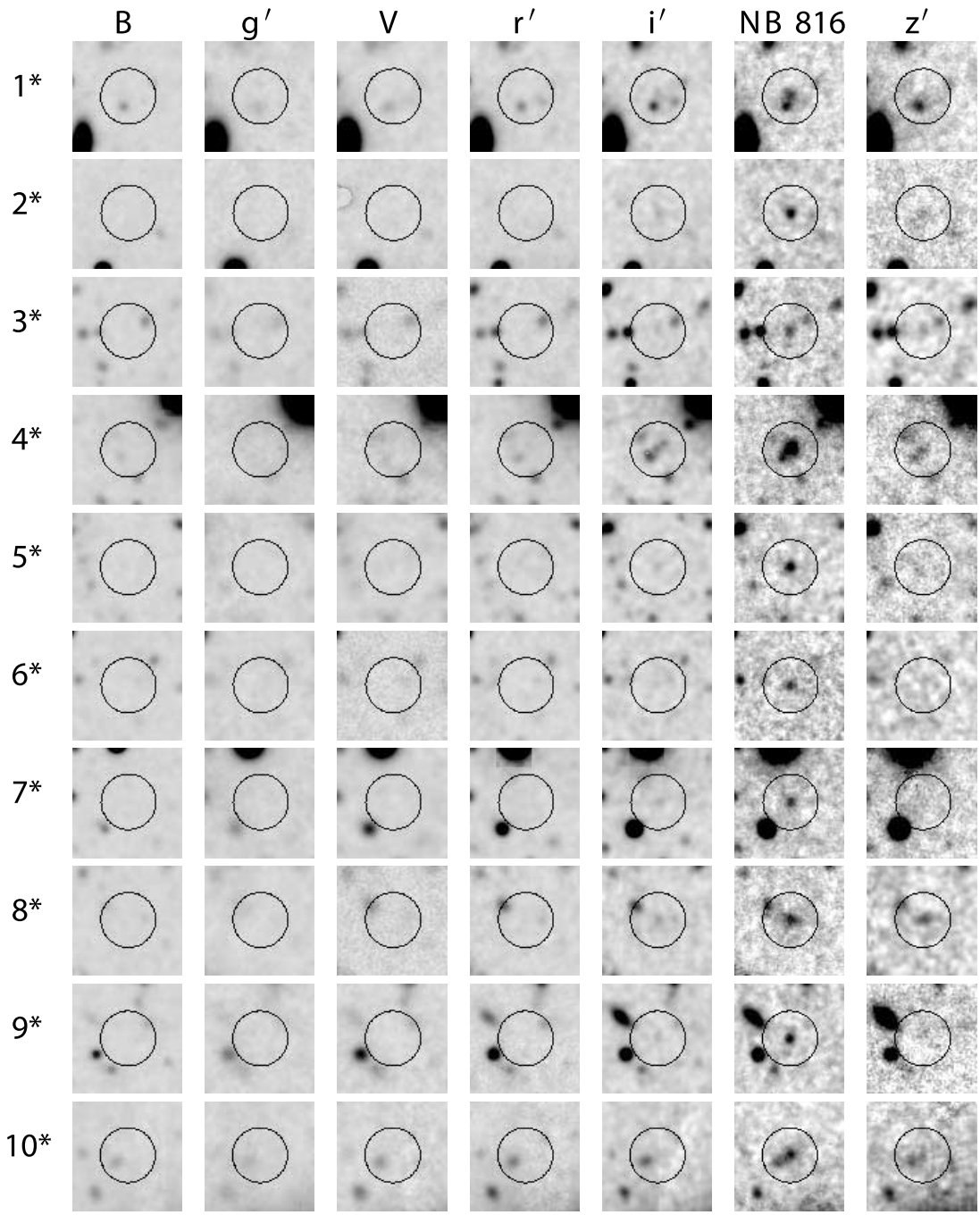

FIG. 2.—Broadband and NB816 images of our LAE candidates at $z \approx 5.7$. Asterisks at the object number denote the statistical sample. Each box is $12''$ on a side (north is up, and east is to the left). Each circle has a $3''$ radius.

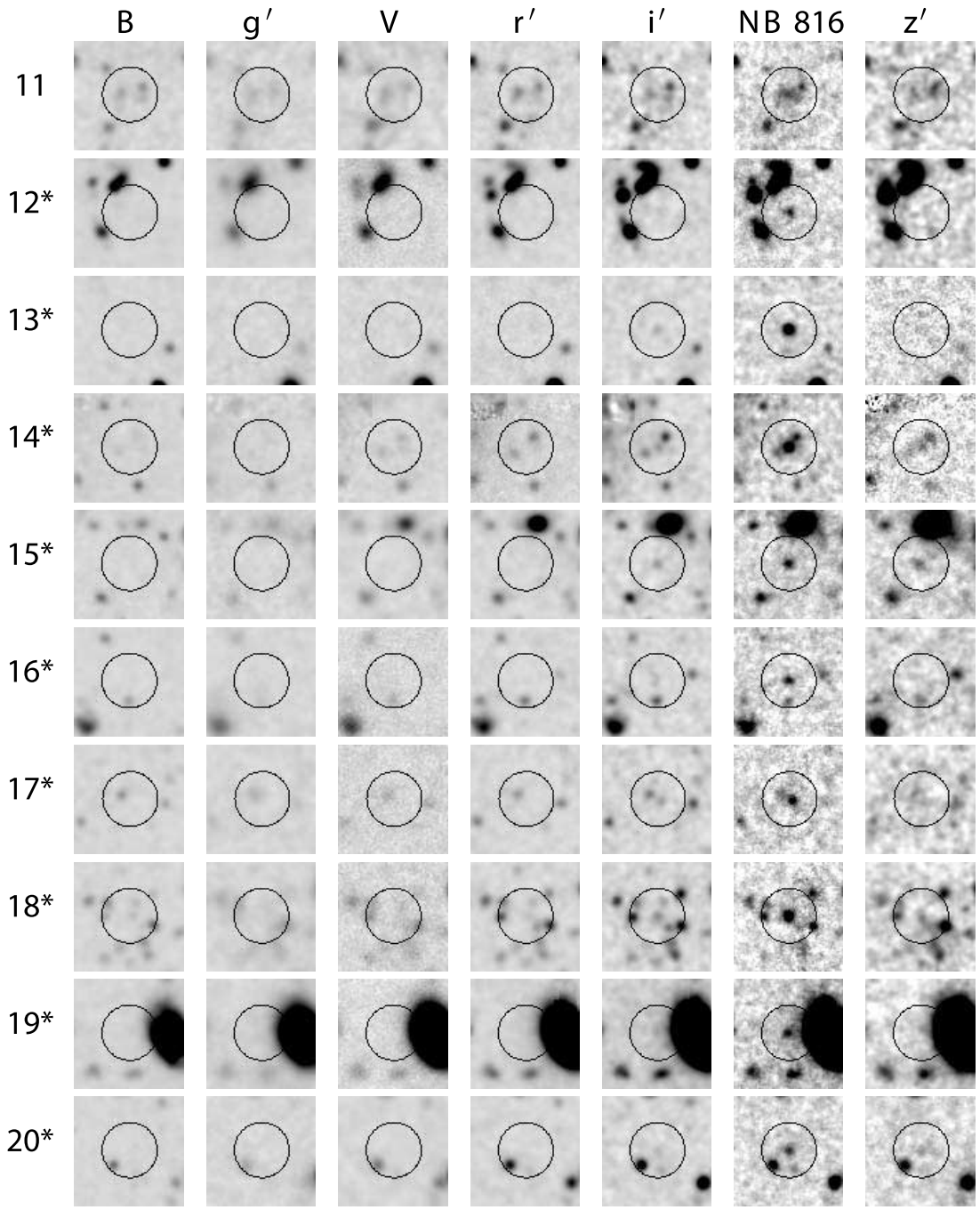

FIG. 2—*Continued*

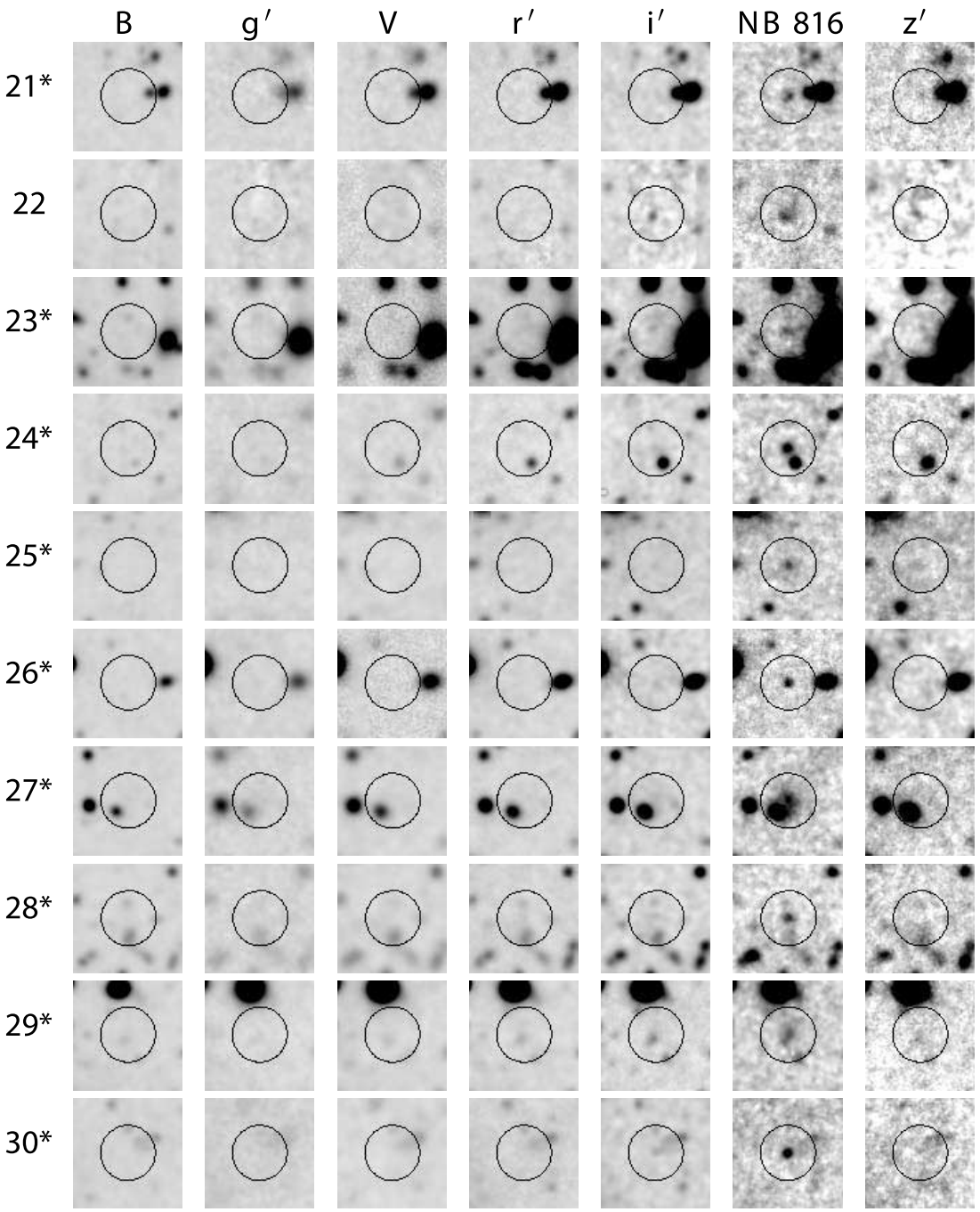

FIG. 2—*Continued*

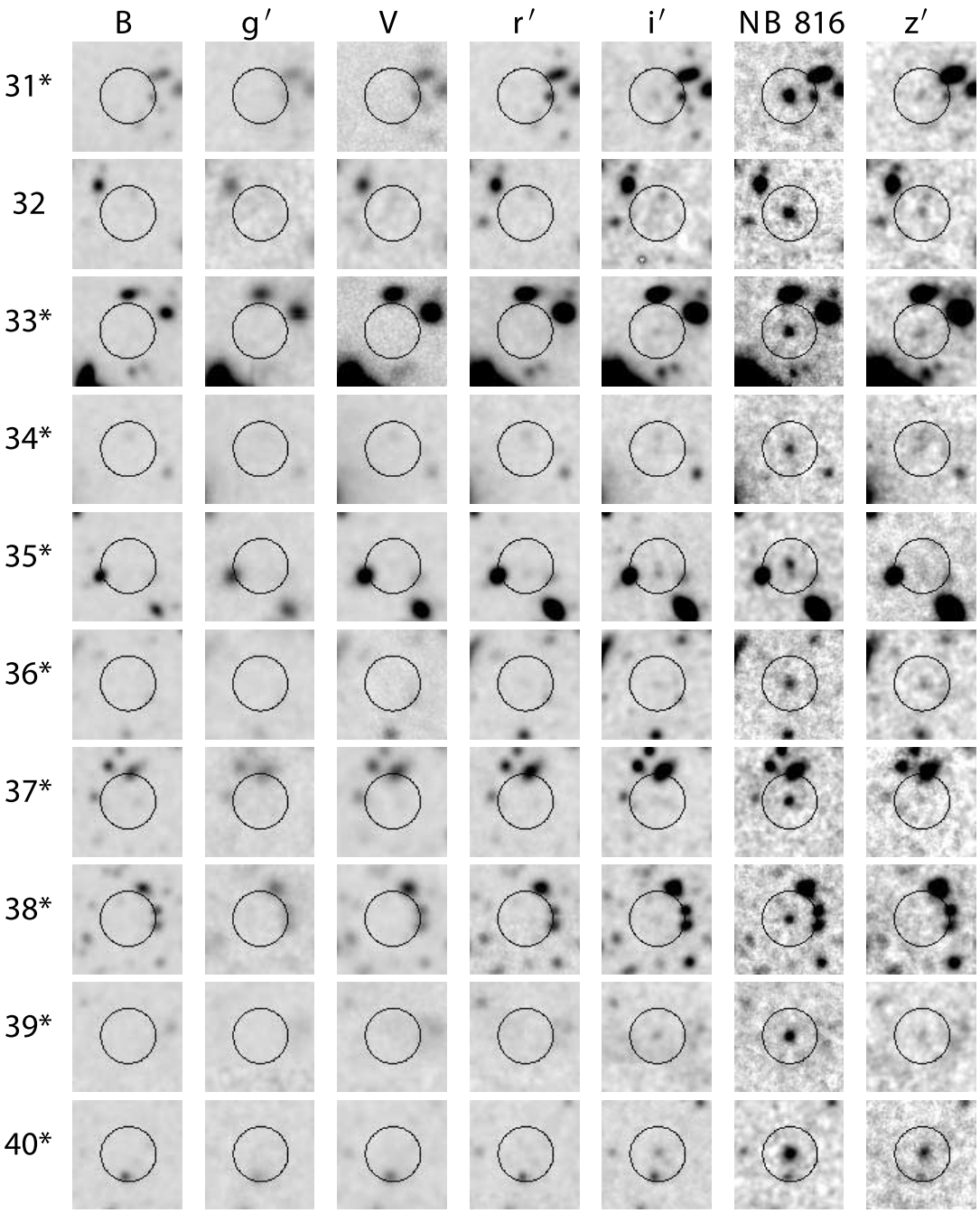

FIG. 2—*Continued*

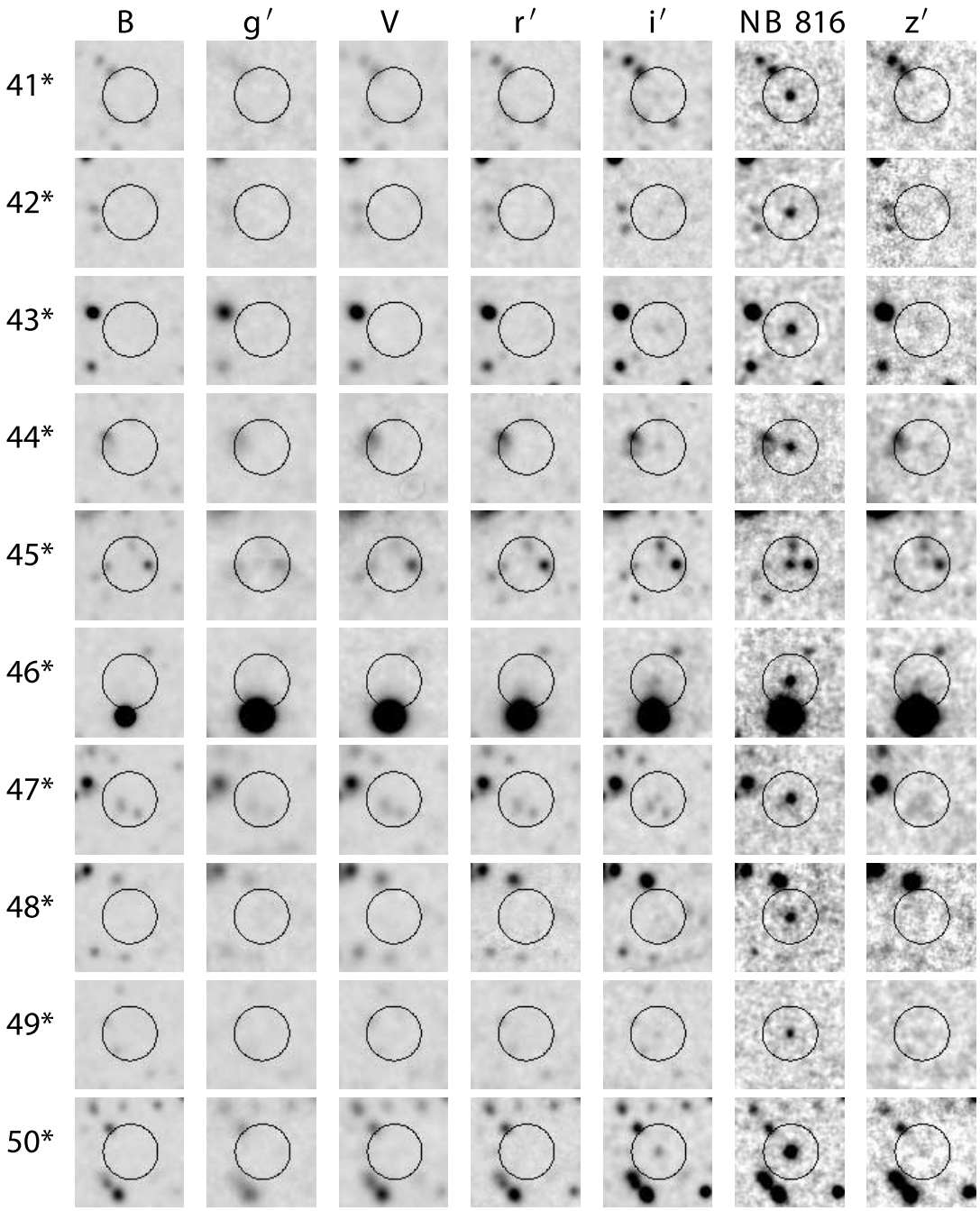

FIG. 2—*Continued*

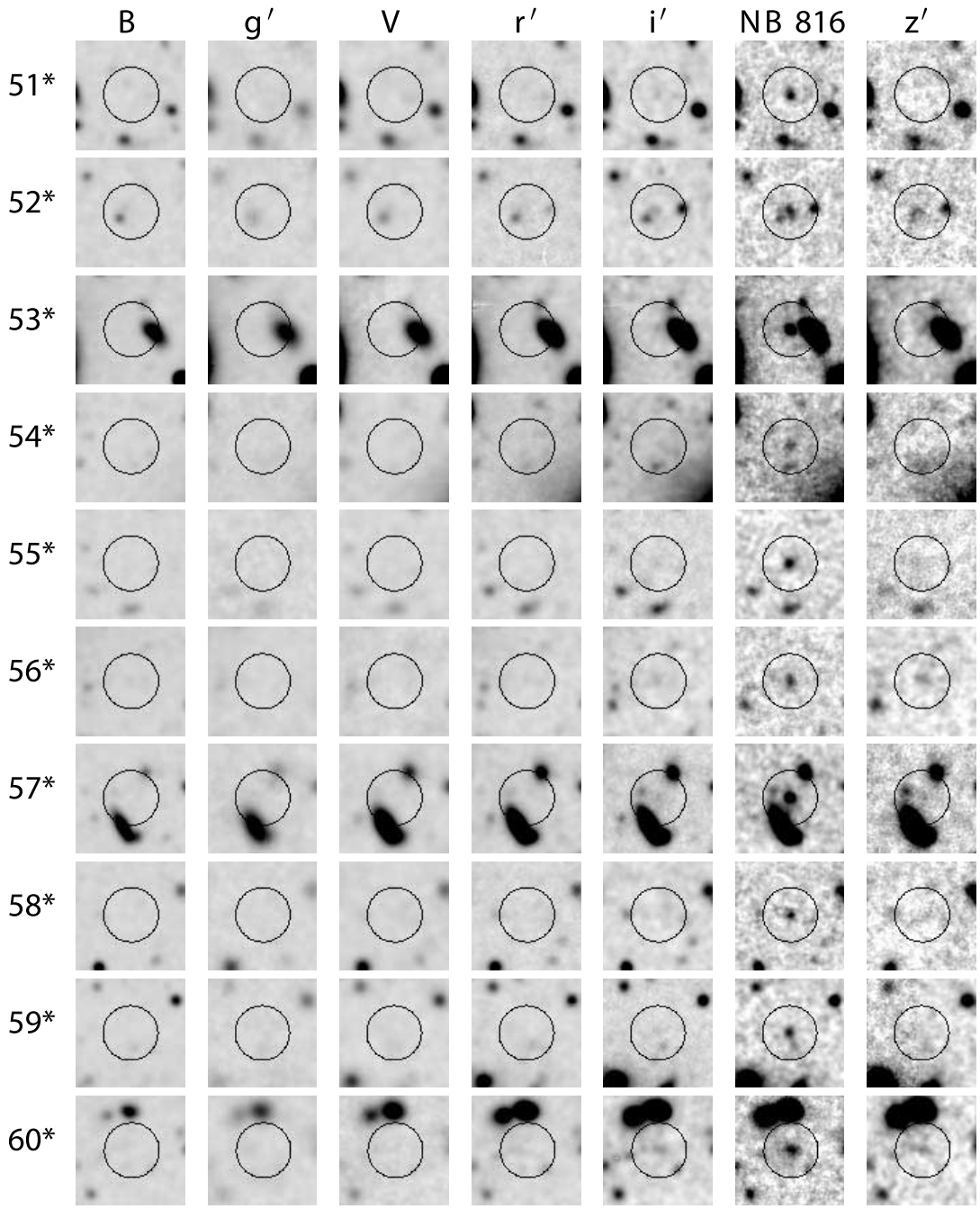

FIG. 2—*Continued*

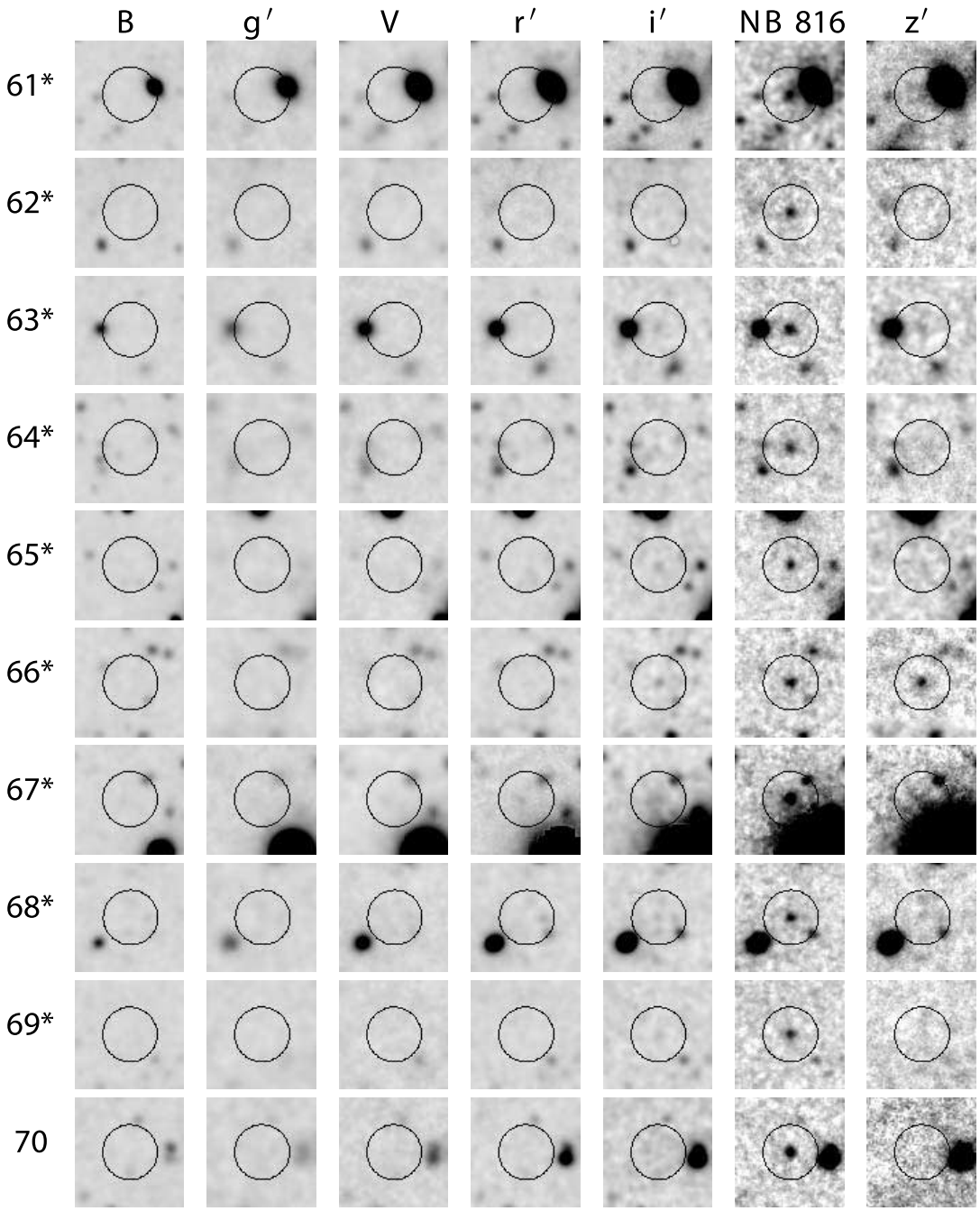

FIG. 2—*Continued*

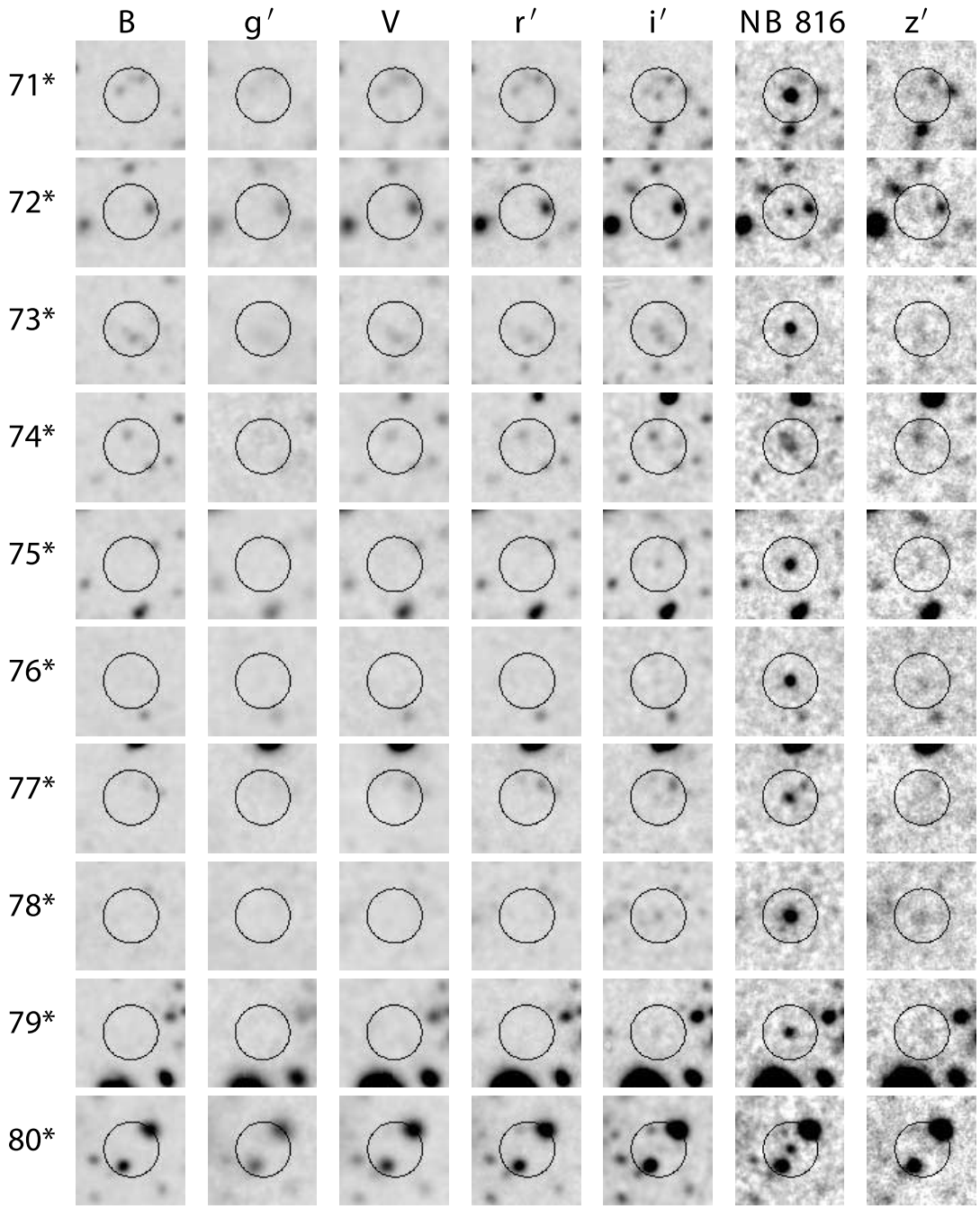

FIG. 2—*Continued*

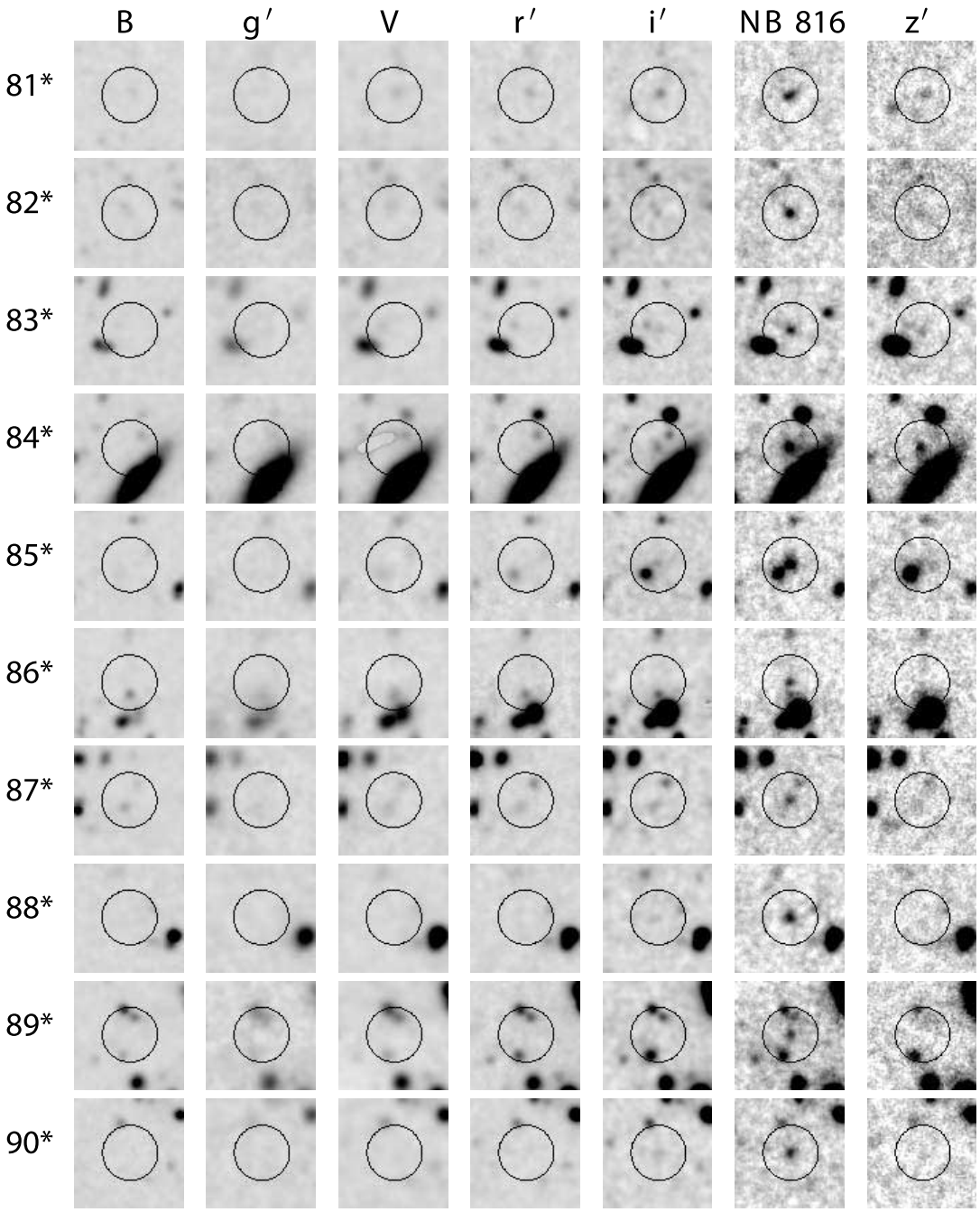

FIG. 2—*Continued*

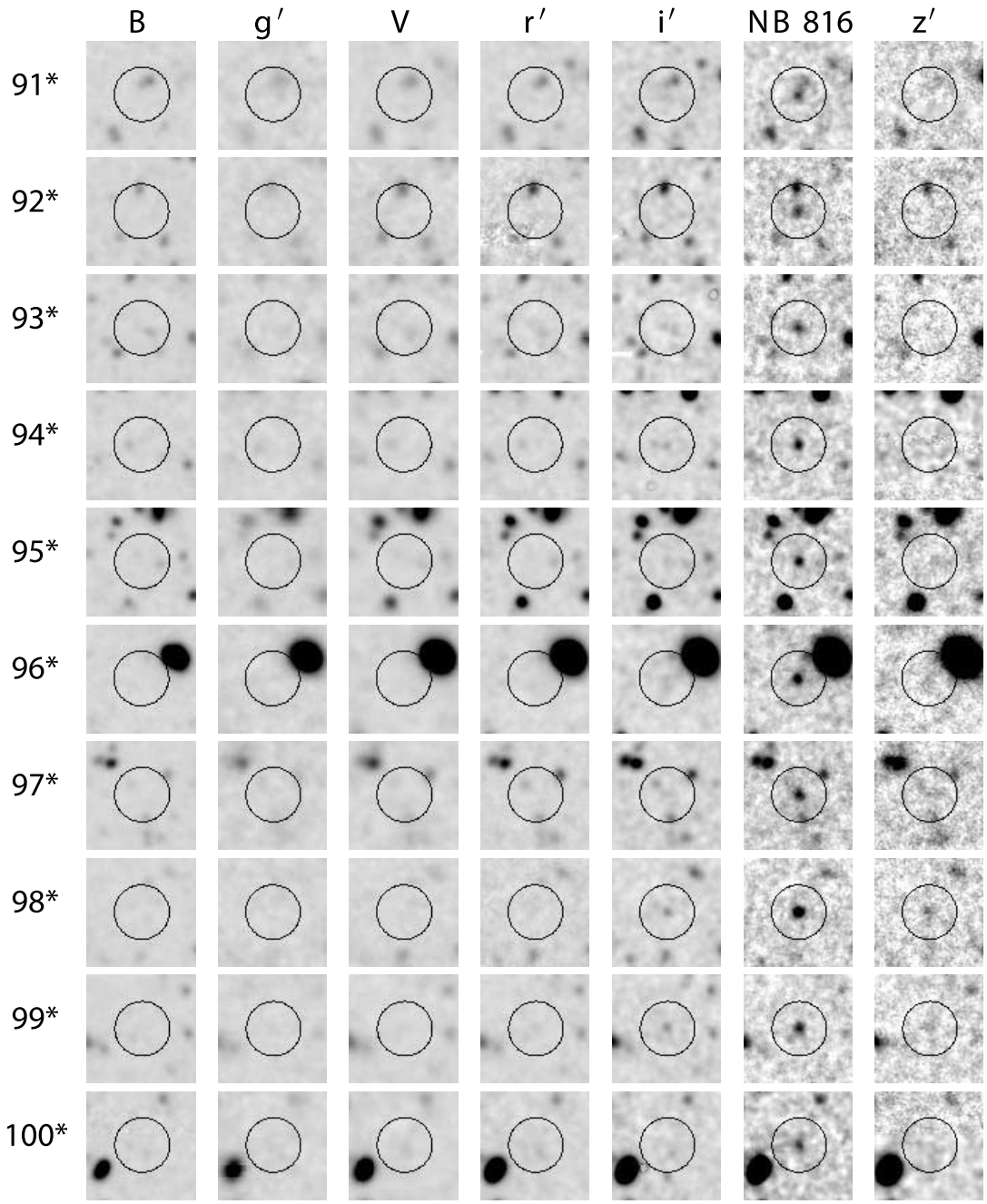

FIG. 2—*Continued*

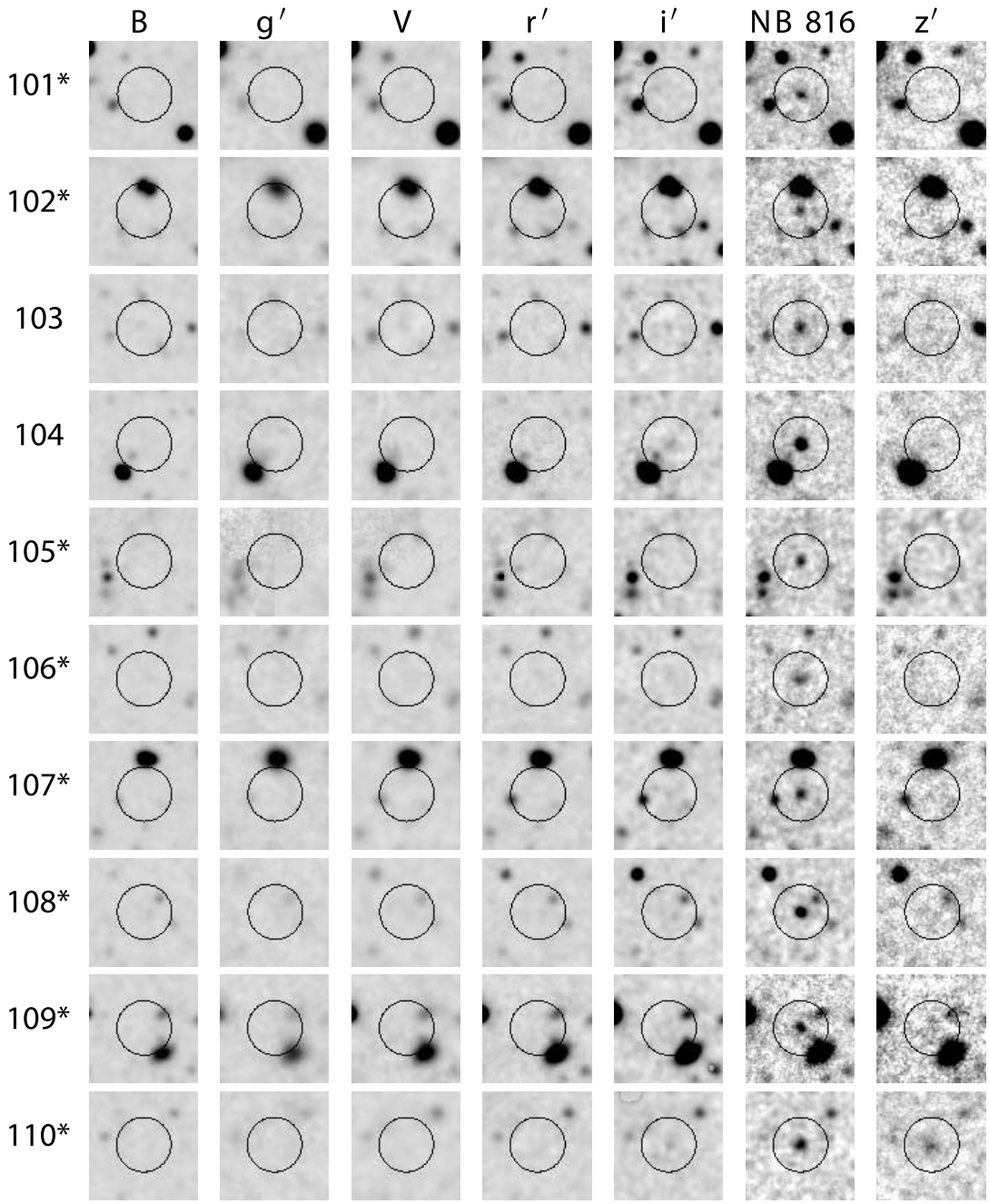

FIG. 2—*Continued*

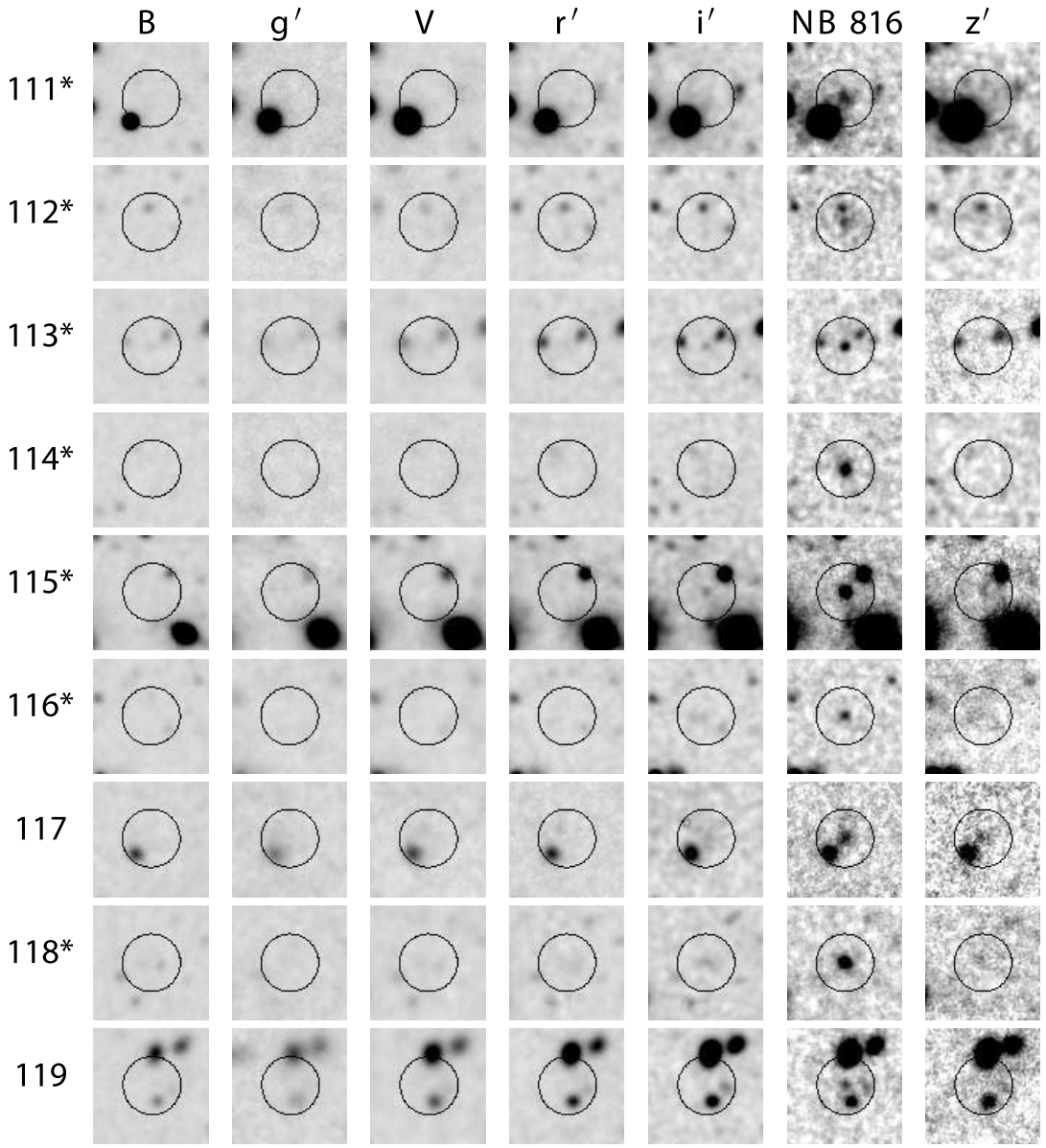

FIG. 2—*Continued*

the magnitude limit of the survey [NB816($2''\phi$) = 25.1], we find $\sim 3 \times 10^5$ sources.

2.2. *Selection of LAE Candidates*

Our main aim in the present survey is to identify reliable LAE candidates at $z \approx 5.7$ by first selecting NB816 excess objects, using the following criteria:

$$\mathrm{NB816}(2''\phi) < 25.1, \quad (1)$$

$$iz(2''\phi) - \mathrm{NB816}(2''\phi) > \max(0.7, 3\sigma_{iz-\mathrm{NB816}}), \quad (2)$$

$$B(0.5''\phi) > 29.6, \quad (3)$$

$$g'(0.5''\phi) > 29.2, \quad (4)$$

$$V(0.5''\phi) > 29.1, \quad (5)$$

$$r'(0.5''\phi) > 29.1, \quad (6)$$

where iz is the continuum magnitude at $\lambda = 8150$ Å, estimated by linear interpolation between i' and z' flux densities ($f_{iz} = 0.57 f_{i'} + 0.43 f_{z'}$). The first criterion ensures that objects are detected above the 5 σ level in the NB816. Criterion (2) allows selection of emission-line objects with observed equivalent width, $\mathrm{EW_{obs}} \geq 120$ Å. The 3 σ of $iz - \mathrm{NB816}$ is estimated from the local-background noise measurement of the most noisy region in the survey area. This is illustrated in Figure 1, where the LAE candidates are identified on $iz - \mathrm{NB816}$ versus NB816 color-magnitude diagram. Criteria (3), (4), (5), and (6) ensure that $z \approx 5.7$ candidates are undetected (at $\approx$1.5 σ noise level) in B, g', V, and r' bands. We adopt magnitudes in a $0.5''$ diameter aperture to avoid possible contamination by low-z foreground objects.

We find a total of 119 LAE candidates at $z \sim 5.7$ that satisfy the above criteria and confirm these by careful eye inspection for apparent false detections (Fig. 2). Our first spectroscopic follow-up observation of $\sim$50 LAE candidates indicates a $\sim$95%

TABLE 1

PHOTOMETRIC PROPERTIES OF THE LAE CANDIDATES AT $z \approx 5.7$

Number[a]	α (J2000.0) (deg)	δ(J2000.0) (deg)	NB816[b] (ϕ2.0″)	i'[b] (ϕ2.0″)	z'[b] (ϕ2.0″)	iz[b] (ϕ2.0″)	NB816[b] (ϕ3.0″)	z'[b] (ϕ3.0″)	f_ν(NB816)[c] (ϕ3.0″)	$f_\nu(z')$[c] (ϕ3.0″)	$f_{\rm line}$[d]	EW$_{\rm obs}$[e] (Å)
1*	149.4786	+2.2116	24.9	26.3	26.4	26.3	24.5	25.9	5.6 ± 0.6	1.6 ± 0.9	2.6 ± 0.4	353 ± 207
2*	149.5460	+2.7640	24.8	26.7	26.0	26.3	24.6	25.9	5.0 ± 0.7	1.6 ± 1.0	2.3 ± 0.5	307 ± 191
3*	149.5790	+1.5183	25.1	26.9	26.2	26.5	24.7	26.3	4.8 ± 0.7	1.1 ± 1.0	2.3 ± 0.5	452 ± 401
4*	149.6052	+2.4476	23.7	25.2	25.3	25.2	23.2	24.8	18.3 ± 0.6	4.3 ± 1.0	8.8 ± 0.4	452 ± 107
5*	149.6320	+2.3466	24.7	27.1	26.7	26.9	24.4	26.2	6.2 ± 0.8	1.2 ± 1.0	3.0 ± 0.5	578 ± 498
6*	149.6331	+1.8223	25.0	27.7	27.3	27.5	24.7	26.4	4.7 ± 0.7	<1.0	2.3 ± 0.5	>498
7*	149.6361	+2.3276	24.9	26.5	26.3	26.4	24.6	25.6	5.2 ± 0.7	2.2 ± 0.9	2.2 ± 0.4	227 ± 105
8*	149.6537	+1.5394	24.7	26.1	25.0	25.5	24.2	24.8	7.4 ± 0.7	4.5 ± 1.0	2.8 ± 0.5	136 ± 39
9*	149.6804	+2.7076	24.8	27.2	27.2	27.2	24.6	30.4	5.4 ± 0.8	<1.0	2.9 ± 0.5	>659
10*	149.6886	+2.9180	24.5	26.0	25.3	25.6	24.1	24.6	8.7 ± 0.7	5.0 ± 1.1	3.3 ± 0.5	147 ± 39
11	149.7334	+1.4765	24.7	25.7	25.5	25.6	24.1	24.8	8.6 ± 0.9	4.5 ± 1.4	3.4 ± 0.6	171 ± 61
12*	149.7362	+1.5594	25.0	27.9	99.0	99.0	24.7	99.0	4.6 ± 0.8	<1.2	2.5 ± 0.5	>463
13*	149.7457	+2.7519	24.1	27.1	27.4	27.2	23.9	99.0	9.6 ± 0.7	<1.0	5.2 ± 0.5	>1172
14*	149.7493	+2.7609	24.1	25.6	25.4	25.5	23.6	25.0	12.9 ± 0.7	3.6 ± 1.0	6.0 ± 0.5	369 ± 105
15*	149.7537	+2.2380	24.8	26.3	25.4	25.8	24.6	25.1	5.1 ± 0.7	3.3 ± 0.9	1.9 ± 0.5	127 ± 47
16*	149.7725	+1.7967	25.1	27.2	27.7	27.4	24.9	27.5	3.9 ± 0.7	<1.0	2.0 ± 0.5	>454
17*	149.7810	+1.5176	24.6	25.9	25.8	25.9	24.2	25.2	7.6 ± 0.9	3.1 ± 1.1	3.3 ± 0.6	237 ± 96
18*	149.7812	+1.4940	24.1	25.8	25.8	25.8	23.8	25.7	10.9 ± 0.9	2.0 ± 1.2	5.4 ± 0.6	612 ± 385
19*	149.8019	+1.8274	24.6	25.7	26.3	25.9	24.2	25.9	7.6 ± 0.7	1.6 ± 1.1	3.7 ± 0.5	517 ± 360
20*	149.8023	+2.2251	25.0	27.0	26.2	26.6	24.7	26.0	4.9 ± 0.6	1.5 ± 1.0	2.2 ± 0.4	344 ± 241
21*	149.8082	+2.6360	25.1	27.5	27.0	27.3	24.8	27.5	4.6 ± 0.8	<1.0	2.4 ± 0.5	>529
22	149.8085	+1.5439	24.8	26.2	26.5	26.4	24.3	99.0	6.7 ± 0.8	<1.6	3.6 ± 0.6	>498
23*	149.8186	+1.7204	25.0	26.1	26.2	26.1	24.4	25.9	6.1 ± 0.7	1.6 ± 1.0	2.8 ± 0.5	387 ± 237
24*	149.8203	+2.7823	24.5	26.6	26.4	26.5	24.3	26.4	6.9 ± 0.7	<1.1	3.5 ± 0.5	>669
25*	149.8323	+2.0561	25.1	26.9	26.5	26.7	24.6	26.7	5.3 ± 0.6	<0.9	2.6 ± 0.4	>633
26*	149.8380	+1.6948	25.1	26.8	30.2	27.4	25.1	28.7	3.5 ± 0.6	<0.9	1.8 ± 0.4	>473
27*	149.8443	+2.7615	24.3	26.2	26.2	26.2	24.0	25.8	9.4 ± 0.5	1.8 ± 0.7	4.6 ± 0.4	571 ± 239
28*	149.8466	+2.7517	25.1	26.8	99.0	99.0	24.8	27.0	4.3 ± 0.6	<0.9	2.2 ± 0.4	>518
29*	149.8776	+2.3317	24.9	25.9	26.4	26.1	24.4	26.0	6.5 ± 0.6	1.4 ± 1.0	3.1 ± 0.4	481 ± 328
30*	149.8893	+2.8322	24.6	26.4	26.8	26.6	24.3	25.8	7.2 ± 0.7	1.7 ± 1.1	3.5 ± 0.5	445 ± 286
31*	149.9107	+1.6147	24.1	26.3	26.0	26.2	23.8	26.2	11.2 ± 0.7	1.2 ± 0.9	5.7 ± 0.4	1031 ± 767
32	149.9197	+1.4827	24.2	26.9	25.8	26.3	23.9	26.1	10.3 ± 0.9	1.4 ± 1.2	5.2 ± 0.6	851 ± 748
33*	149.9303	+1.5980	24.5	26.3	25.4	25.8	24.2	25.1	7.5 ± 0.8	3.5 ± 1.0	3.1 ± 0.5	199 ± 66
34*	149.9336	+2.0141	25.0	26.9	26.0	26.4	24.7	25.5	5.0 ± 0.6	2.4 ± 1.0	2.1 ± 0.4	191 ± 88
35*	149.9422	+2.1286	24.8	26.1	26.0	26.1	24.4	25.6	6.1 ± 0.6	2.1 ± 0.8	2.7 ± 0.4	283 ± 120
36*	149.9447	+1.5357	24.8	27.2	25.9	26.4	24.5	25.9	5.7 ± 0.7	1.6 ± 1.0	2.6 ± 0.5	375 ± 241
37*	149.9586	+2.9017	24.6	27.0	27.4	27.2	24.4	99.0	6.4 ± 0.7	<1.2	3.5 ± 0.5	>667
38*	149.9625	+2.5397	24.8	26.9	30.2	27.5	24.5	99.0	5.6 ± 0.7	<1.0	3.1 ± 0.5	>670
39*	149.9672	+1.6231	24.4	26.2	26.1	26.2	24.2	26.0	7.8 ± 0.6	1.4 ± 0.9	3.8 ± 0.4	596 ± 376
40*	149.9719	+2.1182	24.2	25.9	24.7	25.2	23.9	24.4	10.0 ± 0.6	6.1 ± 1.0	3.8 ± 0.4	137 ± 27
41*	149.9735	+2.8166	24.6	27.2	28.3	27.5	24.5	99.0	5.8 ± 0.7	<1.0	3.2 ± 0.5	>690
42*	149.9772	+2.2546	24.9	27.1	27.1	27.1	24.8	27.3	4.4 ± 0.6	<1.1	2.3 ± 0.4	>479
43*	149.9783	+2.1776	24.5	26.5	26.3	26.4	24.2	26.1	7.5 ± 0.6	1.4 ± 1.0	3.7 ± 0.4	608 ± 436
44*	149.9792	+1.7890	24.6	26.6	26.3	26.5	24.3	26.0	6.8 ± 0.6	1.4 ± 0.9	3.3 ± 0.4	518 ± 339
45*	150.0021	+1.8278	24.8	26.4	26.0	26.2	24.5	25.9	5.8 ± 0.6	1.6 ± 0.9	2.7 ± 0.4	372 ± 225
46*	150.0638	+1.4831	24.2	25.4	25.4	25.4	23.8	24.9	10.7 ± 0.7	4.0 ± 1.0	4.7 ± 0.5	265 ± 75
47*	150.0653	+2.0156	24.4	26.2	25.7	26.0	24.1	25.2	8.6 ± 0.5	3.0 ± 0.9	3.8 ± 0.4	280 ± 86
48*	150.0710	+2.7698	24.5	27.7	27.5	27.6	24.2	99.0	7.7 ± 0.8	<1.1	4.2 ± 0.5	>831
49*	150.0832	+2.0176	25.1	27.1	26.8	27.0	24.8	28.3	4.2 ± 0.6	<0.9	2.3 ± 0.4	>562
50*	150.0937	+2.6843	23.8	26.0	27.5	26.4	23.5	99.0	14.1 ± 0.7	<1.0	7.9 ± 0.5	>1744
51*	150.1005	+2.7901	24.9	27.2	99.0	99.0	24.9	99.0	4.0 ± 0.7	<1.0	2.7 ± 0.5	>592
52*	150.1019	+2.9165	24.6	26.2	25.5	25.8	24.2	25.0	7.3 ± 0.7	3.5 ± 1.1	3.0 ± 0.5	192 ± 69
53*	150.1090	+1.5444	23.9	25.5	25.2	25.4	23.5	24.9	13.9 ± 0.6	4.1 ± 0.9	6.4 ± 0.4	352 ± 84
54*	150.1214	+2.6877	25.1	25.9	99.0	99.0	24.5	26.9	5.8 ± 0.7	<1.0	2.9 ± 0.5	>647
55*	150.1267	+2.2874	24.8	27.3	26.7	27.0	24.5	26.6	5.5 ± 0.6	<0.9	2.8 ± 0.4	>649
56*	150.1335	+1.5006	25.0	26.6	25.8	26.1	24.6	25.9	5.1 ± 0.6	1.6 ± 1.0	2.3 ± 0.4	317 ± 195
57*	150.1376	+2.2597	23.9	25.8	25.5	25.6	23.5	24.9	14.0 ± 0.7	4.2 ± 1.0	6.5 ± 0.4	344 ± 83
58*	150.1566	+2.8614	25.0	28.9	27.7	28.2	24.8	99.0	4.2 ± 0.7	<1.0	2.4 ± 0.5	>523
59*	150.1676	+2.3177	24.9	27.6	27.0	27.3	24.7	26.3	4.9 ± 0.6	1.1 ± 1.0	2.4 ± 0.4	455 ± 413
60*	150.1919	+1.5765	24.5	25.8	25.8	25.8	24.1	25.5	8.3 ± 0.7	2.3 ± 1.0	3.9 ± 0.5	374 ± 174
61*	150.2032	+2.2278	24.3	25.7	25.0	25.3	24.0	24.3	8.9 ± 0.6	6.7 ± 0.9	3.0 ± 0.4	100 ± 19
62*	150.2166	+2.7730	24.8	27.5	99.0	99.0	24.5	99.0	5.7 ± 0.7	<1.1	3.3 ± 0.5	>686
63*	150.2254	+1.5436	24.6	26.5	25.8	26.1	24.2	25.5	7.3 ± 0.7	2.3 ± 1.0	3.3 ± 0.5	320 ± 151
64*	150.2314	+1.6086	24.9	27.6	26.6	27.0	24.5	25.8	5.8 ± 0.6	1.8 ± 0.9	2.6 ± 0.4	326 ± 168

TABLE 1—*Continued*

Number[a]	α (J2000.0) (deg)	δ(J2000.0) (deg)	NB816[b] (ϕ2.0″)	i'[b] (ϕ2.0″)	z'[b] (ϕ2.0″)	iz[b] (ϕ2.0″)	NB816[b] (ϕ3.0″)	z'[b] (ϕ3.0″)	f_ν(NB816)[c] (ϕ3.0″)	$f_\nu(z')$[c] (ϕ3.0″)	$f_{\rm line}$[d]	EW$_{\rm obs}$[e] (Å)
65*	150.2434	+1.6119	25.0	26.6	26.7	26.6	24.8	26.4	4.4 ± 0.6	1.0 ± 0.9	2.1 ± 0.4	456 ± 413
66*	150.2471	+1.5555	24.6	26.5	24.8	25.4	24.3	24.5	6.7 ± 0.7	6.0 ± 1.0	2.0 ± 0.5	75 ± 22
67*	150.2521	+2.8980	23.9	25.4	24.5	24.9	23.3	23.7	17.1 ± 0.7	12.6 ± 1.2	5.9 ± 0.5	104 ± 13
68*	150.2623	+1.8624	24.9	26.9	26.8	26.9	24.5	26.7	5.8 ± 0.6	<0.9	2.9 ± 0.4	>741
69*	150.2807	+1.8730	24.9	27.4	28.4	27.7	24.6	99.0	5.1 ± 0.6	<0.9	2.8 ± 0.4	>679
70	150.2852	+1.4858	24.5	27.0	28.2	27.4	24.3	27.5	6.8 ± 0.8	<1.3	3.6 ± 0.6	>593
71*	150.2905	+2.2538	23.5	25.9	26.0	25.9	23.3	25.3	17.6 ± 0.6	2.8 ± 0.9	8.8 ± 0.4	704 ± 230
72*	150.2973	+2.8944	25.0	27.3	26.7	27.0	24.8	25.8	4.3 ± 0.7	1.7 ± 1.2	1.8 ± 0.5	234 ± 169
73*	150.3267	+1.9511	24.2	25.7	26.1	25.8	24.0	25.7	8.8 ± 0.6	1.9 ± 1.0	4.2 ± 0.4	488 ± 250
74*	150.3400	+2.8002	24.9	26.6	26.0	26.3	24.4	25.6	6.2 ± 0.7	2.1 ± 1.0	2.8 ± 0.5	294 ± 153
75*	150.3493	+1.9334	24.4	26.7	26.2	26.4	24.2	26.0	7.7 ± 0.7	1.4 ± 1.0	3.8 ± 0.5	602 ± 442
76*	150.3621	+1.7417	24.3	28.0	25.9	26.6	24.0	25.6	8.8 ± 0.6	2.2 ± 0.9	4.2 ± 0.4	427 ± 183
77*	150.3657	+2.5017	24.7	26.8	26.2	26.5	24.3	25.6	7.0 ± 0.7	2.0 ± 1.0	3.2 ± 0.5	355 ± 184
78*	150.3712	+1.8250	23.9	26.1	25.4	25.8	23.5	25.0	14.2 ± 0.6	3.5 ± 0.9	6.7 ± 0.4	427 ± 115
79*	150.3795	+2.5183	24.6	27.1	26.7	26.9	24.4	26.1	6.5 ± 0.8	1.3 ± 1.0	3.2 ± 0.5	530 ± 427
80*	150.3978	+2.7734	24.8	26.5	26.4	26.4	24.3	25.5	6.6 ± 0.7	2.2 ± 1.0	3.0 ± 0.5	296 ± 138
81*	150.4005	+1.8018	24.9	25.9	25.8	25.9	24.6	26.4	5.1 ± 0.7	<1.1	2.5 ± 0.5	>510
82*	150.4078	+2.9117	24.8	26.4	25.8	26.1	24.6	25.4	5.2 ± 0.7	2.4 ± 1.1	2.2 ± 0.5	200 ± 104
83*	150.4079	+2.1133	25.0	26.5	25.9	26.2	24.7	25.6	4.8 ± 0.7	2.1 ± 0.9	2.0 ± 0.4	210 ± 103
84*	150.4091	+2.8063	24.1	25.3	24.5	24.9	23.5	24.0	13.9 ± 0.6	9.0 ± 1.0	5.1 ± 0.4	126 ± 17
85*	150.4274	+2.4974	24.1	25.8	25.0	25.4	23.8	24.5	11.5 ± 0.8	5.8 ± 1.0	4.6 ± 0.5	178 ± 37
86*	150.4339	+2.4867	25.0	27.1	27.0	27.0	24.8	26.3	4.6 ± 0.7	1.1 ± 1.1	2.2 ± 0.5	429 ± 419
87*	150.4393	+2.7860	25.1	26.7	26.5	26.6	24.7	25.9	4.8 ± 0.7	1.6 ± 1.0	2.2 ± 0.4	306 ± 199
88*	150.4444	+1.8076	24.7	27.5	99.0	99.0	24.5	99.0	5.6 ± 0.7	<1.0	3.2 ± 0.5	>704
89*	150.4685	+2.7071	25.0	28.1	99.0	99.0	24.5	29.6	5.7 ± 0.7	<1.1	3.1 ± 0.5	>619
90*	150.4766	+1.5314	25.0	26.7	99.0	99.0	24.7	99.0	4.7 ± 0.7	<1.1	2.5 ± 0.5	>523
91*	150.4890	+1.6883	25.1	26.3	28.0	26.8	24.6	29.7	5.2 ± 0.7	<1.0	2.8 ± 0.5	>595
92*	150.4984	+2.8138	25.0	27.5	99.0	99.0	24.7	99.0	5.0 ± 0.8	<1.1	2.7 ± 0.5	>564
93*	150.5114	+2.7640	25.0	27.4	99.0	99.0	24.9	99.0	4.1 ± 0.7	<1.	2.5 ± 0.5	>532
94*	150.5131	+1.6066	25.0	26.6	28.2	27.1	24.8	27.1	4.4 ± 0.7	<1.2	2.3 ± 0.5	>431
95*	150.5362	+2.0874	24.9	27.0	27.2	27.1	24.7	26.9	4.8 ± 0.7	<1.0	2.4 ± 0.5	>532
96*	150.5367	+1.9125	24.5	26.5	26.1	26.3	24.1	25.5	8.2 ± 0.7	2.2 ± 1.0	3.8 ± 0.5	378 ± 167
97*	150.5543	+2.8230	24.7	26.8	26.1	26.4	24.4	25.6	6.4 ± 0.7	2.1 ± 1.0	2.9 ± 0.5	308 ± 153
98*	150.5677	+2.5774	24.2	26.2	25.5	25.9	24.0	25.5	8.9 ± 0.7	2.4 ± 1.0	4.2 ± 0.5	388 ± 175
99*	150.5711	+2.3625	24.9	26.1	26.3	26.2	24.6	26.1	5.2 ± 0.6	1.3 ± 1.0	2.5 ± 0.4	429 ± 339
100*	150.5773	+1.6153	25.1	27.3	27.5	27.4	24.8	26.3	4.2 ± 0.7	1.1 ± 1.1	2.0 ± 0.5	392 ± 389
101*	150.6079	+2.4935	25.0	28.2	99.0	99.0	24.8	99.0	4.4 ± 0.7	<1.0	2.9 ± 0.5	>656
102*	150.6386	+2.3956	25.1	27.1	26.7	26.9	24.7	26.0	4.6 ± 0.7	1.4 ± 1.1	2.1 ± 0.5	337 ± 273
103	150.6596	+2.6453	24.7	27.5	26.6	27.1	24.4	26.1	6.5 ± 0.7	1.3 ± 0.9	3.2 ± 0.5	553 ± 420
104	150.6806	+2.7643	23.9	26.1	26.7	26.3	23.7	26.2	12.3 ± 0.7	1.2 ± 0.9	6.3 ± 0.5	1140 ± 860
105*	150.6927	+1.8712	25.1	99.0	99.0	99.0	25.1	99.0	3.4 ± 0.7	<1.0	1.8 ± 0.5	>398
106*	150.7034	+2.7397	25.0	27.5	99.0	99.0	24.7	99.0	4.9 ± 0.7	<1.0	2.9 ± 0.5	>670
107*	150.7111	+2.2247	24.8	27.0	27.2	27.1	24.6	27.7	5.4 ± 0.6	<1.0	2.8 ± 0.4	>614
108*	150.7150	+2.2342	24.4	26.8	26.8	26.8	24.2	26.1	7.7 ± 0.6	1.3 ± 1.0	3.8 ± 0.4	623 ± 460
109*	150.7475	+2.8532	24.6	26.8	25.8	26.2	24.3	25.3	7.1 ± 0.9	2.8 ± 1.2	3.1 ± 0.6	246 ± 113
110*	150.7548	+2.0434	24.6	26.6	25.1	25.7	24.3	24.7	6.7 ± 0.8	4.8 ± 1.0	2.4 ± 0.5	110 ± 34
111*	150.7576	+1.8365	24.4	25.8	25.1	25.4	23.9	24.3	10.1 ± 0.8	7.0 ± 1.2	3.6 ± 0.5	114 ± 25
112*	150.7722	+1.8614	25.1	27.3	26.5	26.9	24.6	26.0	5.3 ± 0.7	1.4 ± 1.1	2.5 ± 0.5	396 ± 325
113*	150.7747	+2.1644	24.9	26.1	99.0	99.0	24.6	99.0	5.4 ± 0.7	<1.1	3.0 ± 0.5	>617
114*	150.7756	+1.7953	24.3	27.0	99.0	99.0	24.0	99.0	9.5 ± 0.7	<1.1	5.1 ± 0.5	>1040
115*	150.7863	+2.6448	23.7	25.4	25.2	25.3	23.4	24.6	16.2 ± 0.8	5.4 ± 1.0	7.3 ± 0.5	304 ± 58
116*	150.7906	+2.2222	25.0	26.8	26.2	26.5	24.7	25.4	4.6 ± 0.7	2.6 ± 1.0	1.8 ± 0.5	151 ± 71
117	150.8054	+2.9250	24.5	25.8	25.1	25.4	24.1	24.8	8.1 ± 1.0	4.3 ± 1.5	3.2 ± 0.7	165 ± 65
118*	150.8211	+2.2498	24.0	26.0	25.8	25.9	23.6	25.5	13.0 ± 0.7	2.3 ± 1.1	6.4 ± 0.5	631 ± 304
119	150.8342	+2.3398	25.0	27.0	26.4	26.7	24.5	25.2	5.8 ± 0.8	3.1 ± 1.3	2.3 ± 0.6	164 ± 79

[a] Asterisks denote the statistical sample.
[b] AB magnitude. An entry of 99.0 indicates that no excess flux was measured. All of our LAE candidates are undetected in the *B*-, g'-, *V*-, and r'-band data.
[c] Flux densities of the NB816 band and the z' band in unit of 10^{-30} ergs s^{-1} cm^{-2} Hz^{-1}. Errors and upper limits represent 1 σ significance.
[d] Estimated line fluxes in unit of 10^{-17} ergs s^{-1} cm^{-2}. Errors represent 1 σ significance.
[e] Estimated observed equivalent widths. Errors and lower limits represent 1 σ significance.

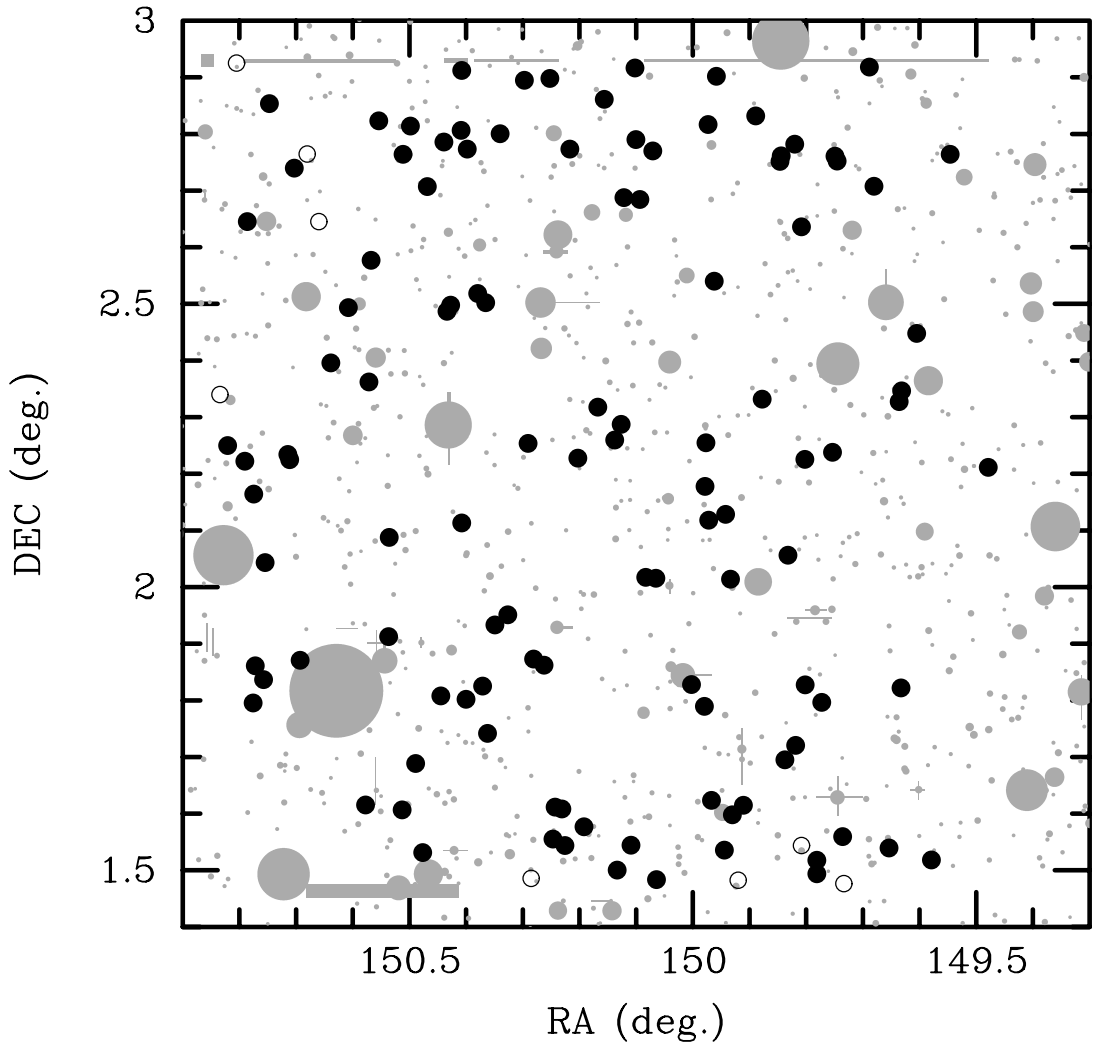

FIG. 3.—Spatial distributions of our 119 LAE candidates. The nonstatistical sample is shown by open circles. The shadowed regions show the areas masked out for the detection.

or better confirmation rate (P. Capak et al. 2007, in preparation). We also find that there is no low-luminosity radio-loud AGN with $L(1.4\ \mathrm{GHz}) > 6 \times 10^{24}\ \mathrm{W\ Hz^{-1}}$ among our final LAE candidates (Carilli et al. 2007). The coordinates and photometric data for the LAE candidates are listed in Table 1. All magnitudes are corrected for Galactic extinction; $\bar{E}(B - V) = 0.0195$ (Capak et al. 2007). In Table 1 we also list emission line fluxes and observed equivalent widths estimated from NB816 and z' flux densities in a $3''$ aperture.

As shown by criterion (2), the detection limit of LAEs depends on the depth of both the NB816 and i' and z' band images. However, we did not impose any noise threshold on the i' and z' band images when we selected the LAE candidates. To ensure homogeneity, we make a subsample of the LAE candidates in areas with low noise, both in the i' and z' bands, where the 5 σ limiting magnitude over a $2''$ diameter aperture is brighter than 25.4 or 24.8 mag in i' and z' bands, respectively. This subsample (hereafter, the statistical sample) contains 111 LAE candidates, which are identified by asterisks in Table 1. We use this "statistical sample" to estimate statistical properties of LAEs, including their number density and luminosity function. The size of the effective area corresponding to this statistical sample is reduced to 1.86 deg^2, equivalent to 3.7×10^4 Mpc^2 of the transverse comoving area at $z = 5.7$. The survey volume for the statistical sample is 1.7×10^6 Mpc^3.

3. RESULTS AND DISCUSSION

3.1. *Spatial Distribution and Angular Two-Point Correlation Function*

In Figure 3, we show the spatial distribution of all the LAE candidates in our sample. There appears to be little evidence for strong clustering. When dividing the survey area into four tiles with $0.7^\circ \times 0.7^\circ$ each, we find 26, 28, 26, and 31 LAEs in the SW, NW, SE, and NE quadrant, respectively. Therefore, the 111 LAE candidates in the statistical sample are almost randomly distributed at least on large scales.

We derive the angular two-point correlation function (ACF), $\omega(\theta)$, for the 111 LAE candidates in the "statistical sample" using the estimator defined by Landy & Szalay (1993),

$$w(\theta) = \frac{DD(\theta) - 2DR(\theta) + RR(\theta)}{RR(\theta)}, \qquad (7)$$

where $DD(\theta)$, $DR(\theta)$, and $RR(\theta)$ are normalized numbers of galaxy-galaxy, galaxy-random, and random-random pairs, respectively. The random sample consists of 100,000 sources with the same geometrical constraints as the LAE sample.

In Figure 4 (*left*), we show the ACF for the statistical LAE sample (*large filled circles*). There is a clustering signal with 2.8 σ

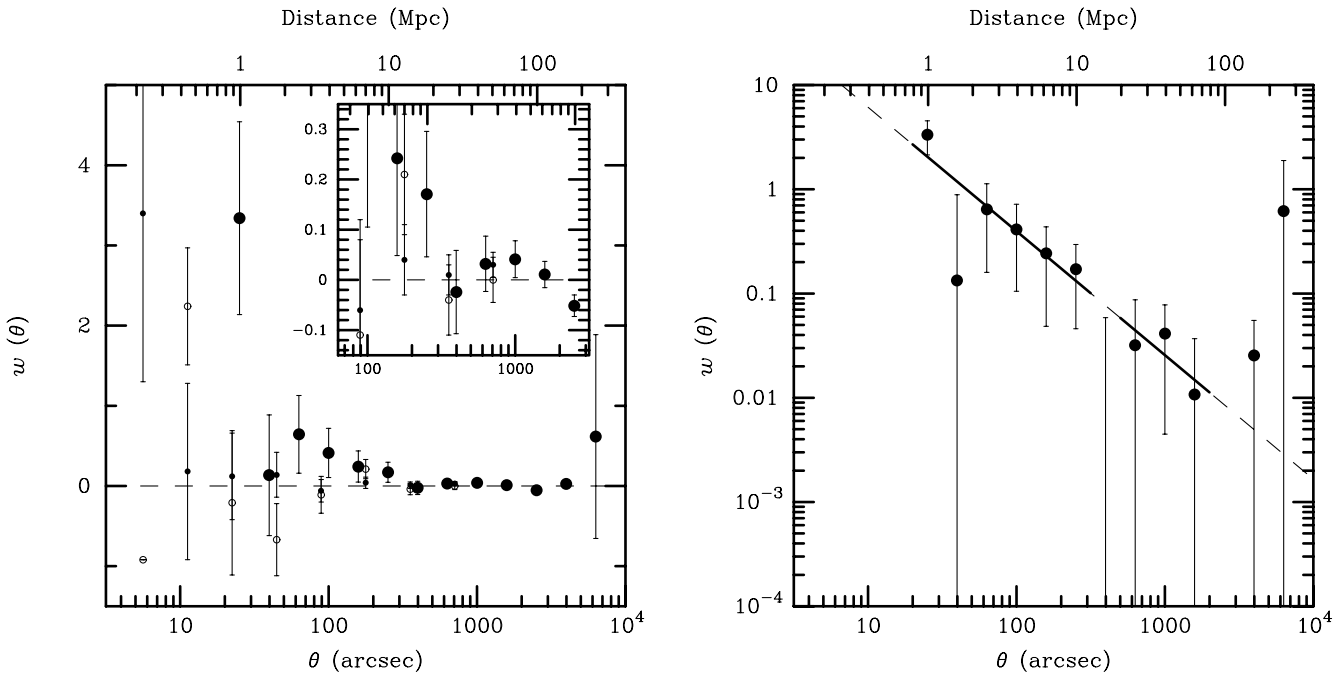

FIG. 4.—*Left*: Angular two-point correlation function of the 111 LAE candidates in the statistical sample (*large filled circles*). The small filled circles correspond to the bright sample (NB816 $\leq$ 25.5) of Shimasaku et al. (2006), while the open circles show the whole sample (NB816 $\leq$ 26.5) of Shimasaku et al. (2006). Note that the NB816 limit of our LAE candidates is 25.1. The inset shows an expanded view at $60'' \leq \theta \leq 3000''$. *Right*: Same as the left panel but $w(\theta)$ is shown by logarithmic scale. Large filled circles show the angular two-point correlation function by the 111 LAE candidates in the statistical sample. The dashed line shows the result of power-law fit of the data points at $25'' \leq \theta \leq 1585''$ except the point at $398''$ (*fitting region shown by the solid line*).

significance at $25''$ ($\simeq$1.0 Mpc at $z = 5.7$). We also find possible signals at $63''$, $100''$, $158''$, and $251''$, although their detection significance is as low as $\simeq 1.3\ \sigma$. We compare this with the ACF for LAE candidates at $z \approx 5.7$ in the SDF (Shimasaku et al. 2006) using their whole sample; NB816 $\leq$ 26.5 (*small filled circles*) and their bright sample; NB816 $\leq$ 25.5 (*open circles*). Most of data points are consistent within 1 σ errors among the three samples. However, there seems to be possible difference among the three samples at small angular scales. Since our LAE sample is limited at NB816 $<$ 25.1, the brighter sample seems to show the larger $w(\theta)$ at $\theta \leq 30''$.

Although the clustering signals are not high, particularly at larger scales (e.g., $\theta \geq 100''$), the LAE candidates in the COSMOS field follow a power-law relation between $w(\theta)$ and θ, as shown in the right panel [i.e., $w(\theta) = A_w \theta^{\beta}$]. We find a best-fit power law with an index of $\beta = -1.2 \pm 0.2$ and an amplitude at $1''$ of $A_w = 95 \pm 76$. For this power-law fit, we only used data points between $25''$ and $1585''$ except the point at $398''$. The value of β is steeper than $\beta = -0.74$ (at $z = 4$) and $\beta = -0.81$ (at $z = 5$) found for Lyman break galaxies in the SDF (Kashikawa et al. 2006). The semianalytic models predict that the ACF for higher halo mass has a steeper slope and a stronger amplitude (Kashikawa et al. 2006), our results imply that the LAEs are embedded in massive dark matter halo, e.g., heavier than $10^{12}\ M_{\odot}$ (Ouchi et al. 2004). However, absence of significant clustering signal for LAEs at $z \approx 5.7$ in the SDF (Shimasaku et al. 2006) may be indicative of cosmic variance in these studies.

3.2. Lyα *Luminosities of LAE Candidates*

Using our total sample of LAE candidates at $z \approx 5.7$ and a volume of 1.7×10^6 Mpc^3, we estimate a space density of $n(\mathrm{Ly}\alpha) \approx 6.6 \times 10^{-5}$ Mpc^{-3} for the LAE candidates in our "statistical sample." This is a factor of 1.6 lower than those in previous LAE surveys with nearly the same NB816 limits (NB816 $\approx$ 25) (Ajiki et al. 2003; Hu et al. 2004). The observed difference is likely caused by cosmic variance.

We measure the Lyα luminosity, $L(\mathrm{Ly}\alpha)$, of our LAE candidates, assuming all the LAEs to be at $z = 5.70$. The rest-frame equivalent widths and Lyα luminosities as listed in Table 2. We adopted aperture magnitudes measured over a $3''$ aperture diameter for estimation of the Lyα luminosity. We find that the magnitudes measured over $2''$ and $3''$ apertures are well correlated with a small systematic offset. However, the total magnitudes from SExtractor (MAGAUTO) show large scatter when compared with the aperture magnitudes measured over $2''$ and $3''$ diameter apertures due to contamination by neighboring objects. The derived Lyα luminosities range from $\approx 6.3 \times 10^{42}$ to $\approx 3.1 \times 10^{43}$ ergs s^{-1}.

Using the 111 LAE candidates in our "statistical sample," we constructed the Lyα luminosity function, as shown in the left panel of Figure 5. We compare this with other Lyα luminosity functions at $z \sim 5.7$ (Rhoads & Malhotra 2001; Ajiki et al. 2003, 2006a; Hu et al. 2004). Our survey has a luminosity limit of $L_{\mathrm{lim}}(\mathrm{Ly}\alpha) = 6.3 \times 10^{42}$ ergs s^{-1}, corresponding to a LAE with NB816 = 25.1, undetected in i' and in z'. This limit is similar to those in Ajiki et al. (2003) and Hu et al. (2004). The luminosity functions do not show any significant difference at the luminous part [$L(\mathrm{Ly}\alpha) \geq 10^{43}$ ergs s^{-1}], although the number density of Rhoads & Malhotra (2001) is smaller compared to those in other surveys. Because of the improved Poisson statistics in the COSMOS LAE sample, the error bars in this survey are relatively smaller. Therefore, the brighter part of the LAE luminosity function is relatively well established. Also, the wide area covered by the COSMOS survey enables us to improve the statistics at the brighter part of the luminosity function [$L(\mathrm{Ly}\alpha) > 2 \times 10^{43}$ ergs s^{-1}] by increasing the number of luminous LAEs per luminosity bin compared to

TABLE 2

Lyα Luminosity and Star Formation Rate for the LAE Candidates at $z \approx 5.7$

Number[a]	$EW_0(Ly\alpha)$[b] (Å)	$L(Ly\alpha)$[b] (10^{42} ergs s^{-1})	$SFR(Ly\alpha)$[b] ($M_\odot$ yr^{-1})	L_{1270}[b,c] (10^{28} ergs s^{-1} Hz^{-1})	SFR(UV)[b] ($M_\odot$ yr^{-1})	SFR(<Lyα)/SFR(UV)[b]
1*	53 ± 31	9.2 ± 1.4	8.4 ± 1.3	8.7 ± 4.9	12.1 ± 6.8	0.69 ± 0.41
2*	46 ± 29	8.0 ± 1.6	7.3 ± 1.5	8.7 ± 5.1	12.1 ± 7.2	0.60 ± 0.38
3*	68 ± 60	8.2 ± 1.6	7.4 ± 1.5	6.0 ± 5.2	8.4 ± 7.2	0.89 ± 0.79
4*	67 ± 16	31.0 ± 1.6	28.2 ± 1.4	22.7 ± 5.2	31.8 ± 7.3	0.89 ± 0.21
5*	86 ± 74	10.7 ± 1.7	9.7 ± 1.6	6.1 ± 5.2	8.6 ± 7.3	1.14 ± 0.98
6*	>74	8.1 ± 1.7	7.4 ± 1.6	<5.4	<7.5	>0.98
7*	34 ± 16	7.9 ± 1.6	7.2 ± 1.4	11.5 ± 4.8	16.1 ± 6.8	0.45 ± 0.21
8*	20 ± 6	9.8 ± 1.7	9.0 ± 1.6	24.0 ± 5.5	33.6 ± 7.7	0.27 ± 0.08
9*	>98	10.4 ± 1.7	9.4 ± 1.6	<5.2	<7.3	>1.29
10*	22 ± 6	11.8 ± 1.8	10.8 ± 1.6	26.6 ± 5.8	37.2 ± 8.1	0.29 ± 0.08
11	25 ± 9	12.2 ± 2.2	11.1 ± 2.0	23.6 ± 7.2	33.1 ± 10.1	0.34 ± 0.12
12*	>69	8.8 ± 1.9	8.0 ± 1.7	<6.3	<8.8	>0.91
13*	>175	18.4 ± 1.6	16.8 ± 1.5	<5.2	<7.3	>2.30
14*	55 ± 16	21.2 ± 1.7	19.3 ± 1.5	19.0 ± 5.2	26.6 ± 7.3	0.72 ± 0.21
15*	19 ± 7	6.7 ± 1.6	6.1 ± 1.5	17.4 ± 4.9	24.3 ± 6.9	0.25 ± 0.09
16*	>68	7.1 ± 1.7	6.4 ± 1.5	<5.1	<7.2	>0.89
17*	35 ± 14	11.7 ± 2.0	10.6 ± 1.8	16.3 ± 6.0	22.8 ± 8.3	0.47 ± 0.19
18*	91 ± 57	19.1 ± 2.1	17.4 ± 1.9	10.3 ± 6.4	14.4 ± 8.9	1.20 ± 0.76
19*	77 ± 54	13.0 ± 1.7	11.9 ± 1.5	8.3 ± 5.7	11.7 ± 8.0	1.02 ± 0.71
20*	51 ± 36	8.0 ± 1.5	7.2 ± 1.4	7.7 ± 5.2	10.7 ± 7.2	0.68 ± 0.47
21*	>79	8.4 ± 1.8	7.6 ± 1.6	<5.2	<7.3	>1.04
22	>74	12.8 ± 2.1	11.7 ± 1.9	<8.5	<11.9	>0.98
23*	58 ± 35	10.1 ± 1.6	9.2 ± 1.5	8.6 ± 5.1	12.0 ± 7.1	0.76 ± 0.47
24*	>100	12.3 ± 1.7	11.2 ± 1.6	<6.1	<8.5	>1.32
25*	>94	9.3 ± 1.4	8.5 ± 1.3	<4.9	<6.8	>1.24
26*	>71	6.5 ± 1.5	5.9 ± 1.3	<4.5	<6.4	>0.93
27*	85 ± 36	16.3 ± 1.3	14.8 ± 1.1	9.4 ± 3.9	13.2 ± 5.4	1.12 ± 0.47
28*	>77	7.6 ± 1.5	7.0 ± 1.4	<4.9	<6.8	>1.02
29*	72 ± 49	11.1 ± 1.4	10.1 ± 1.3	7.6 ± 5.1	10.7 ± 7.1	0.95 ± 0.64
30*	66 ± 43	12.2 ± 1.7	11.1 ± 1.5	9.1 ± 5.7	12.7 ± 8.0	0.87 ± 0.56
31*	154 ± 114	20.3 ± 1.5	18.5 ± 1.4	6.5 ± 4.8	9.1 ± 6.7	2.03 ± 1.51
32	127 ± 112	18.5 ± 2.1	16.8 ± 2.0	7.2 ± 6.3	10.1 ± 8.8	1.67 ± 1.47
33*	30 ± 10	11.0 ± 1.8	10.0 ± 1.6	18.3 ± 5.3	25.6 ± 7.5	0.39 ± 0.13
34*	29 ± 13	7.3 ± 1.5	6.6 ± 1.3	12.6 ± 5.2	17.6 ± 7.3	0.38 ± 0.17
35*	42 ± 18	9.6 ± 1.3	8.7 ± 1.2	11.2 ± 4.5	15.7 ± 6.2	0.56 ± 0.24
36*	56 ± 36	9.4 ± 1.6	8.5 ± 1.5	8.3 ± 5.1	11.6 ± 7.2	0.74 ± 0.47
37*	>100	12.4 ± 1.8	11.3 ± 1.6	<6.1	<8.6	>1.31
38*	>100	10.9 ± 1.7	9.9 ± 1.5	<5.4	<7.5	>1.32
39*	89 ± 56	13.6 ± 1.4	12.3 ± 1.3	7.5 ± 4.7	10.5 ± 6.6	1.17 ± 0.74
40*	20 ± 4	13.3 ± 1.5	12.1 ± 1.4	32.3 ± 5.1	45.2 ± 7.1	0.27 ± 0.05
41*	>103	11.2 ± 1.7	10.2 ± 1.5	<5.3	<7.5	>1.36
42*	>72	8.0 ± 1.6	7.3 ± 1.4	<5.5	<7.8	>0.94
43*	91 ± 65	13.2 ± 1.5	12.0 ± 1.3	7.2 ± 5.1	10.0 ± 7.1	1.20 ± 0.86
44*	77 ± 51	11.6 ± 1.5	10.6 ± 1.4	7.4 ± 4.8	10.4 ± 6.7	1.02 ± 0.67
45*	55 ± 34	9.6 ± 1.5	8.8 ± 1.3	8.6 ± 5.0	12.0 ± 7.0	0.73 ± 0.44
46*	39 ± 11	16.7 ± 1.7	15.2 ± 1.6	20.9 ± 5.5	29.3 ± 7.7	0.52 ± 0.15
47*	42 ± 13	13.5 ± 1.3	12.3 ± 1.2	15.9 ± 4.6	22.3 ± 6.5	0.55 ± 0.17
48*	>124	14.8 ± 1.8	13.5 ± 1.6	<5.9	<8.2	>1.63
49*	>84	8.0 ± 1.4	7.3 ± 1.2	<4.7	<6.6	>1.11
50*	>260	27.9 ± 1.6	25.4 ± 1.5	<5.3	<7.4	>3.43
51*	>88	9.5 ± 1.7	8.7 ± 1.5	<5.3	<7.4	>1.16
52*	29 ± 10	10.7 ± 1.8	9.7 ± 1.6	18.4 ± 5.9	25.8 ± 8.2	0.38 ± 0.14
53*	53 ± 13	22.8 ± 1.5	20.7 ± 1.4	21.4 ± 4.9	30.0 ± 6.9	0.69 ± 0.17
54*	>97	10.4 ± 1.7	9.5 ± 1.5	<5.3	<7.5	>1.27
55*	>97	9.8 ± 1.5	8.9 ± 1.3	<5.0	<7.0	>1.28
56*	47 ± 29	8.2 ± 1.5	7.5 ± 1.4	8.6 ± 5.0	12.0 ± 7.1	0.62 ± 0.38
57*	51 ± 12	22.8 ± 1.6	20.8 ± 1.4	22.0 ± 5.1	30.8 ± 7.2	0.68 ± 0.16
58*	>78	8.5 ± 1.7	7.8 ± 1.5	<5.4	<7.6	>1.03
59*	68 ± 62	8.3 ± 1.5	7.6 ± 1.4	6.1 ± 5.4	8.5 ± 7.6	0.89 ± 0.81
60*	56 ± 26	13.7 ± 1.7	12.5 ± 1.5	12.1 ± 5.5	17.0 ± 7.6	0.73 ± 0.34
61*	15 ± 3	10.7 ± 1.5	9.7 ± 1.3	35.2 ± 4.8	49.3 ± 6.7	0.20 ± 0.04
62*	>102	11.5 ± 1.7	10.5 ± 1.6	<5.6	<7.8	>1.35
63*	48 ± 23	11.8 ± 1.6	10.8 ± 1.5	12.2 ± 5.5	17.1 ± 7.7	0.63 ± 0.30
64*	49 ± 25	9.4 ± 1.4	8.5 ± 1.3	9.5 ± 4.7	13.3 ± 6.6	0.64 ± 0.33

TABLE 2—*Continued*

Number[a]	$EW_0(Ly\alpha)$[b] (Å)	$L(Ly\alpha)$[b] (10^{42} ergs s^{-1})	$SFR(Ly\alpha)$[b] ($M_\odot$ yr^{-1})	L_{1270}[b,c] (10^{28} ergs s^{-1} Hz^{-1})	SFR(UV)[b] ($M_\odot$ yr^{-1})	SFR(<Lyα)/SFR(UV)[b]
65*	68 ± 62	7.4 ± 1.4	6.7 ± 1.3	5.3 ± 4.7	7.5 ± 6.6	0.90 ± 0.81
66*	11 ± 3	7.1 ± 1.7	6.5 ± 1.5	31.5 ± 5.3	44.1 ± 7.5	0.15 ± 0.04
67*	15 ± 2	20.8 ± 1.8	18.9 ± 1.6	66.3 ± 6.3	92.9 ± 8.9	0.20 ± 0.03
68*	>111	10.4 ± 1.4	9.4 ± 1.3	<4.6	<6.5	>1.46
69*	>101	10.0 ± 1.4	9.1 ± 1.3	<4.9	<6.8	>1.33
70	>89	12.6 ± 2.0	11.5 ± 1.8	<7.0	<9.8	>1.17
71*	105 ± 34	31.1 ± 1.4	28.3 ± 1.3	14.6 ± 4.7	20.5 ± 6.6	1.38 ± 0.45
72*	35 ± 25	6.5 ± 1.8	5.9 ± 1.6	9.2 ± 6.2	12.9 ± 8.7	0.46 ± 0.33
73*	73 ± 37	15.0 ± 1.5	13.7 ± 1.4	10.2 ± 5.1	14.2 ± 7.2	0.96 ± 0.49
74*	44 ± 23	9.9 ± 1.7	9.0 ± 1.6	11.1 ± 5.4	15.5 ± 7.6	0.58 ± 0.30
75*	90 ± 66	13.4 ± 1.6	12.2 ± 1.5	7.4 ± 5.3	10.3 ± 7.4	1.18 ± 0.87
76*	64 ± 27	14.8 ± 1.4	13.5 ± 1.3	11.5 ± 4.8	16.0 ± 6.7	0.84 ± 0.36
77*	53 ± 27	11.5 ± 1.6	10.5 ± 1.5	10.7 ± 5.3	15.0 ± 7.4	0.70 ± 0.36
78*	64 ± 17	23.8 ± 1.4	21.7 ± 1.3	18.4 ± 4.8	25.8 ± 6.8	0.84 ± 0.23
79*	79 ± 64	11.2 ± 1.9	10.2 ± 1.7	7.0 ± 5.5	9.8 ± 7.7	1.04 ± 0.84
80*	44 ± 21	10.6 ± 1.7	9.6 ± 1.5	11.8 ± 5.2	16.5 ± 7.2	0.58 ± 0.27
81*	>76	8.9 ± 1.7	8.1 ± 1.6	<5.7	<8.0	>1.00
82*	30 ± 15	7.7 ± 1.8	7.0 ± 1.6	12.7 ± 5.9	17.8 ± 8.3	0.39 ± 0.20
83*	31 ± 15	7.1 ± 1.6	6.5 ± 1.4	11.2 ± 4.9	15.7 ± 6.9	0.41 ± 0.20
84*	19 ± 3	18.1 ± 1.5	16.5 ± 1.4	47.5 ± 5.1	66.5 ± 7.1	0.25 ± 0.03
85*	27 ± 5	16.4 ± 1.8	14.9 ± 1.6	30.5 ± 5.3	42.7 ± 7.4	0.35 ± 0.07
86*	64 ± 63	7.7 ± 1.6	7.0 ± 1.5	5.9 ± 5.6	8.3 ± 7.9	0.84 ± 0.82
87*	46 ± 30	7.8 ± 1.6	7.1 ± 1.4	8.4 ± 5.2	11.7 ± 7.3	0.60 ± 0.39
88*	>105	11.4 ± 1.7	10.4 ± 1.5	<5.3	<7.5	>1.38
89*	>92	10.8 ± 1.8	9.8 ± 1.6	<5.8	<8.1	>1.22
90*	>78	9.0 ± 1.7	8.2 ± 1.5	<5.7	<8.0	>1.03
91*	>89	9.9 ± 1.7	9.0 ± 1.5	<5.5	<7.7	>1.17
92*	>84	9.5 ± 1.8	8.7 ± 1.6	<5.6	<7.8	>1.11
93*	>79	8.8 ± 1.7	8.0 ± 1.5	<5.5	<7.7	>1.05
94*	>64	8.0 ± 1.7	7.3 ± 1.6	<6.1	<8.6	>0.85
95*	>79	8.5 ± 1.6	7.7 ± 1.5	<5.3	<7.4	>1.05
96*	56 ± 25	13.5 ± 1.7	12.3 ± 1.5	11.8 ± 5.0	16.5 ± 7.0	0.74 ± 0.33
97*	46 ± 23	10.2 ± 1.6	9.3 ± 1.5	10.9 ± 5.1	15.3 ± 7.2	0.61 ± 0.30
98*	58 ± 26	14.8 ± 1.7	13.4 ± 1.6	12.6 ± 5.5	17.6 ± 7.7	0.76 ± 0.34
99*	64 ± 51	8.7 ± 1.5	7.9 ± 1.4	6.7 ± 5.2	9.4 ± 7.3	0.84 ± 0.67
100*	58 ± 58	7.1 ± 1.7	6.4 ± 1.6	6.0 ± 5.7	8.3 ± 8.0	0.77 ± 0.76
101*	>98	10.2 ± 1.7	9.3 ± 1.5	<5.1	<7.2	>1.29
102*	50 ± 41	7.6 ± 1.7	6.9 ± 1.6	7.4 ± 5.7	10.4 ± 8.0	0.66 ± 0.54
103	83 ± 63	11.2 ± 1.6	10.2 ± 1.5	6.7 ± 5.0	9.3 ± 6.9	1.09 ± 0.82
104	170 ± 128	22.3 ± 1.7	20.3 ± 1.5	6.5 ± 4.9	9.1 ± 6.8	2.24 ± 1.69
105*	>59	6.5 ± 1.6	5.9 ± 1.5	<5.4	<7.6	>0.78
106*	>100	10.2 ± 1.6	9.3 ± 1.5	<5.0	<7.1	>1.32
107*	>92	10.1 ± 1.6	9.2 ± 1.4	<5.4	<7.6	>1.21
108*	93 ± 69	13.4 ± 1.5	12.2 ± 1.4	7.1 ± 5.2	9.9 ± 7.2	1.23 ± 0.90
109*	37 ± 17	10.9 ± 2.0	9.9 ± 1.8	14.6 ± 6.1	20.4 ± 8.6	0.48 ± 0.22
110*	16 ± 5	8.4 ± 1.9	7.6 ± 1.7	25.1 ± 5.4	35.2 ± 7.6	0.22 ± 0.07
111*	17 ± 4	12.6 ± 1.9	11.5 ± 1.7	36.8 ± 6.1	51.5 ± 8.5	0.22 ± 0.05
112*	59 ± 48	8.8 ± 1.7	8.0 ± 1.6	7.4 ± 5.9	10.3 ± 8.2	0.78 ± 0.64
113*	>92	10.5 ± 1.7	9.6 ± 1.5	<5.6	<7.9	>1.21
114*	>155	18.1 ± 1.8	16.5 ± 1.6	<5.8	<8.1	>2.04
115*	45 ± 9	26.0 ± 1.7	23.6 ± 1.6	28.3 ± 5.1	39.6 ± 7.1	0.60 ± 0.11
116*	23 ± 11	6.3 ± 1.6	5.7 ± 1.5	13.8 ± 5.4	19.3 ± 7.6	0.30 ± 0.14
117	25 ± 10	11.4 ± 2.3	10.4 ± 2.1	22.9 ± 7.7	32.1 ± 10.8	0.32 ± 0.13
118*	94 ± 45	22.8 ± 1.7	20.7 ± 1.5	11.9 ± 5.7	16.7 ± 8.0	1.24 ± 0.60
119	25 ± 12	8.2 ± 2.0	7.5 ± 1.8	16.5 ± 6.9	23.1 ± 9.6	0.32 ± 0.16

[a] Asterisks denote the statistical sample.
[b] Errors and lower limits represent 1 σ significance.
[c] The UV continuum luminosity at $\lambda = 1270$ Å.

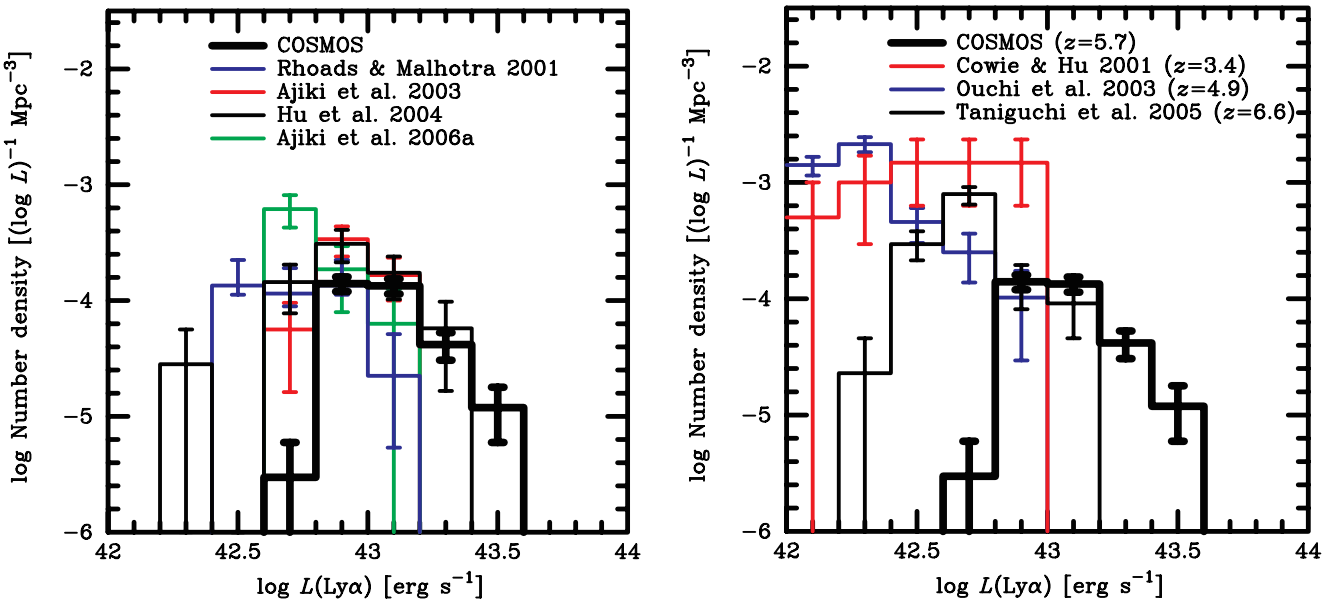

FIG. 5.—Lyα luminosity functions for our LAE candidates. *Left*: Our result (*thick line*) is compared with those from previous surveys for LAEs at $z \sim 5.7$ (Rhoads & Malhotra 2001; Ajiki et al. 2003, 2006a; Hu et al. 2004). *Right*: Our result (*thick line*) is compared with those from previous surveys for LAEs at $z = 3.4$ (Cowie & Hu 1998), $z = 4.9$ (Ouchi et al. 2003), and $z = 6.6$ (Taniguchi et al. 2005).

previous surveys. Note that Westra et al. (2006) explored the LAE luminosity function at $L(\mathrm{Ly}\alpha) = 10^{43.3}$–$10^{43.4}$ ergs s^{-1} with good statistics. The number density from their survey at this brightest luminosity range is similar to that of this study. At $10^{42.8} \leq L(\mathrm{Ly}\alpha) < 10^{43.0}$ ergs s^{-1}, the number density from this study is almost the same as that of Rhoads & Malhotra (2001) and Ajiki et al. (2006a) while smaller (by a factor of 2) than that estimated in Hu et al. (2004) and Ajiki et al. (2003). This is, at least partly, due to both spatial variance and incompleteness at $10^{42.8} \leq L(\mathrm{Ly}\alpha) < 10^{43.0}$ ergs s^{-1} in our survey.

In Figure 5 (*right panel*), we also compare our result with those of previous LAE surveys as a function of redshift. The LAE luminosity functions at $z = 3.4$, 4.9, and 6.6 are taken from Cowie & Hu (1998), Ouchi et al. (2003), and Taniguchi et al. (2005), respectively. COSMOS ($z = 5.7$) and Taniguchi et al. 2005 ($z = 6.6$) give almost the same result within errors at the bright end [$L(\mathrm{Ly}\alpha) \geq 10^{43}$ ergs s^{-1}]. No LAE with $L(\mathrm{Ly}\alpha) \geq 10^{43}$ ergs s^{-1} is found in the previous LAE surveys at $z = 3.4$ and 4.9. While there are differences on the detection completeness and the contamination rates among the surveys, this may provide evidence for the number and/or luminosity evolutions of LAEs.

3.3. *Star Formation Rates*

We now estimate the contribution from LAEs to the star formation rate (SFR) at $z \approx 5.7$, using the following relation (Kennicutt 1998; Brocklehurst 1971),

$$\mathrm{SFR}(<\mathrm{Ly}\alpha) = 9.1 \times 10^{-43} L(\mathrm{Ly}\alpha)\ M_\odot\ \mathrm{yr}^{-1}, \qquad (8)$$

where $L(\mathrm{Ly}\alpha)$ is in ergs s^{-1}. We assume Salpeter initial mass function with $(m_{\mathrm{lower}},\ m_{\mathrm{upper}}) = (0.1\ M_\odot,\ 100\ M_\odot)$.

The estimated SFRs are given in the fourth column of Table 2. They range from 5.7 to 28.3 $M_\odot$ yr^{-1} with a median value of 9.6 $M_\odot$ yr^{-1}. The SFRs derived here can be underestimated due to the effect of absorption by H I gas both in the host galaxies and in the intergalactic medium and dusts in the host galaxies. SFRs independent of the absorption are estimated by the radio data; an upper limit to the mean massive SFR (5–100 $M_\odot$) for the LAE sample is derived as $\sim$100 $M_\odot$ yr^{-1} (Carilli et al. 2007).

The estimated SFRs from the Lyα luminosities here are comparable to those of LAEs at $z \simeq 5.7$–6.6 (e.g., Ajiki et al. 2003; Taniguchi et al. 2005). The SFR density at $z = 5.7$ is estimated by summing up the Lyα luminosities of the 111 "statistical candidates" and corresponds to 7.2×10^{-4} $M_\odot$ yr^{-1} Mpc^{-3}, similar to those obtained in previous narrowband surveys.

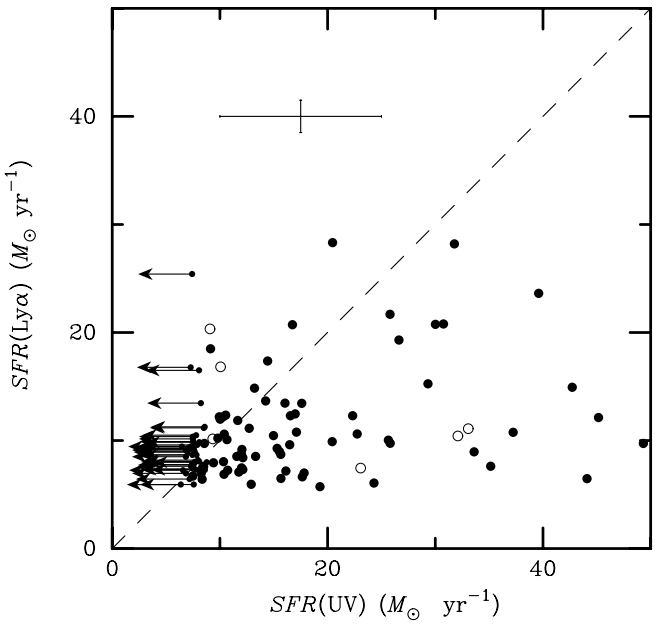

FIG. 6.—Comparison between SFR(Lyα) and SFR(UV) for our 119 LAE candidates. The nonstatistical sample is shown by open circles. The dashed line shows the relation of SFR(Lyα)/SFR(UV) = 1. The cross bar in top left shows the typical 1 σ error for our LAE candidates.

It would be instructive to examine whether the SFRs derived from the Lyα luminosity here are consistent with those based on the UV continuum luminosity from the broadband data. The observed z' magnitudes, measured over 3″ aperture diameters, are converted to UV continuum luminosities at $\lambda = 1270$ Å and used to estimate the SFRs, using the relation (Kennicutt 1998; see also Madau et al. 1998)

$$\mathrm{SFR(UV)} = 1.4 \times 10^{-28} L_\nu \, M_\odot \, \mathrm{yr}^{-1}, \quad (9)$$

where L_ν is the UV continuum luminosity in ergs s^{-1} Hz^{-1}. For each object, we estimate the SFR from its rest-frame UV ($\lambda = 1270$ Å) continuum luminosity, with the results summarized in Table 2. Comparison between SFR(Lyα) and SFR(UV) in Figure 6 shows that, on average, SFR(UV) is relatively higher than SFR(Lyα) for most of the LAE candidates. We find an average ratio of $\mathrm{SFR_{total}(Ly\alpha)/SFR_{total}(UV)} = 0.68$, where $\mathrm{SFR_{total}(Ly\alpha)}$ and $\mathrm{SFR_{total}(UV)}$ are, respectively, the sum of SFRs of all our 119 LAE candidates from Lyα line and UV continuum. The relatively lower SFR(Lyα) compared to SFR(UV) is likely due to the effect of the differential absorption. However, some of our LAE candidates have SFR(Lyα)/SFR(UV) > 1; e.g., those ratios of candidates 13, 27, 50, 71, and 114 are greater than unity with 2 σ significance. They may be in a very early phase ($<10^8$ yr) of star formation activity in which SFR(UV) is underestimated (Schaerer 2000; see also Nagao et al. 2004, 2005).

4. SUMMARY

We have presented results from our narrowband deep imaging survey of the COSMOS field, targeting LAEs at $z \approx 5.7$. This is the largest contiguous survey of LAEs. Our main results are summarized below:

1. We found 119 LAE candidates in our narrowband survey. Allowing for changes in the noise level over the entire field, we extracted a subsample of 111 LAEs that is used to make our statistical analysis.
2. We find no significant evidence for clustering of LAEs at $z \sim 5.7$ contrary to some of the previous LAE surveys.
3. An analysis of angular two-point correlation function gives the power-law relation $w(\theta) = A_w \theta^\beta$, with $\beta = -1.2 \pm 0.2$. The power-law index here is steeper than that found for Lyman break galaxies at $z = 4$ and 5. This suggests that LAEs at $z \approx 5.7$ might be located in massive dark matter halos with mass of $>10^{12} M_\odot$.
4. The number density of LAEs and the average star formation rate are similar to those measured in previous surveys. We estimate a star formation rate (SFR) density of $\sim 7 \times 10^{-4} M_\odot$ yr^{-1} Mpc^{-3} at $z \approx 5.7$.
5. We measure the Lyα luminosity function at $z > 5$ and extend this to $L(\mathrm{Ly\alpha}) \geq 10^{43.5}$ ergs s^{-1}. We compare the estimated Lyα luminosity function here with those in previous studies in the range $z = 3.4$–6.6.

We would like to thank both the Subaru and *HST* staff for their invaluable help. We also thank Masami Ouchi for providing us his data. This work was financially supported in part by the Ministry of Education, Culture, Sports, Science, and Technology (10044052 and 10304013), and by JSPS (15340059 and 17253001). S. S. S. and T. N. are JSPS fellows.

REFERENCES

Ajiki, M., Mobasher, B., Taniguchi, Y., Shioya, Y., Nagao, T., Murayama, T., & Sasaki, S. S. 2006a, ApJ, 638, 596
Ajiki, M., et al. 2003, AJ, 126, 2091
———. 2006b, PASJ, 58, 499
Bertin, E., & Arnouts, S. 1996, A&AS, 117, 393
Bouwens, R. J., & Illingworth, G. D. 2006, Nature, 443, 189
Brocklehurst, M. 1971, MNRAS, 153, 471
Capak, P., et al. 2007, ApJS, 172, 99
Carilli, C. L., et al. 2007, ApJS, 172, 518
Cowie, L. L., & Hu, E. M. 1998, AJ, 115, 1319
Hu, E. M., Cowie, L. L., Capak, P., McMahon, R. G., Hayashino, T., & Komiyama, Y. 2004, AJ, 127, 563
Hu, E. M., & McMahon, R. G. 1996, Nature, 382, 281
Iwata, I., Ohta, K., Tamura, N., Ando, M., Wada, S., Watanabe, C., Akiyama, M., & Aoki, K. 2003, PASJ, 55, 415
Iye, M., et al. 2004, PASJ, 56, 381
Kaifu, N., et al. 2000, PASJ, 52, 1
Kashikawa, N., et al. 2006, ApJ, 637, 631
Kennicutt, R. C., Jr. 1998, ARA&A, 36, 189
Koekemoer, A., et al. 2007, ApJS, 172, 196
Landy, S., & Szalay, A. S. 1993, ApJ, 412, 64
Madau, P., Pozzetti, L., & Dickinson, M. 1998, ApJ, 498, 106
Miyazaki, S., et al. 2002, PASJ, 54, 833
Nagao, T., et al. 2004, ApJ, 613, L9
———. 2005, ApJ, 634, 142
Ouchi, M., et al. 2003, ApJ, 582, 60
———. 2004, ApJ, 611, 685
———. 2005, ApJ, 620, L1
Overzier, R. A., et al. 2006, ApJ, 637, 58
Rhoads, J. E., & Malhotra, S. 2001, ApJ, 563, L5
Schaerer, D. 2000, in Building the Galaxies, ed. F. Hammer et al. (Gif-sur-Yvette: Editions Frontières), 389
Scoville, N. Z., et al. 2007, ApJS, 172, 1
Sekiguchi, K., et al. 2004, Ap&SS Library, 301, 169
Shimasaku, K., et al. 2004, ApJ, 605, L93
———. 2006, PASJ, 58, 313
Steidel, C. C., Adelberger, K. L., Giavalisco, M., Dickinson, M., & Pettini, M. 1999, ApJ, 519, 1
Taniguchi, Y., et al. 2005, PASJ, 57, 165
———. 2007, ApJS, 172, 9
Venemans, B. P., et al. 2002, ApJ, 569, L11
———. 2004, A&A, 424, L17
Westra, E., et al. 2006, A&A, 455, 61
Zheng, W., et al. 2006, ApJ, 640, 574